INVESTIGATIONS OF THE PUP-PROTEASOME SYSTEM IN MYCOBACTERIUM TUBERCULOSIS

Christa Schiesswohl

A thesis

submitted in partial fulfillment of the

requirements for the degree of

Master of Science

University of Washington

2016

Committee:

Champak Chatterjee, Chair

Robert Synovec

Program Authorized to Offer Degree:

Chemistry

University of Washington

Abstract

INVESTIGATIONS OF THE PUP-PROTEASOME SYSTEM IN MYCOBACTERIUM TUBERCULOSIS

Christa Schiesswohl

Chair of the Supervisory Committee:
Champak Chatterjee, Ph.D.
Chemistry

Protein degradation via the proteasome is essential for full virulence of the pathogen *Mycobacterium tuberculosis*. The enzyme PafA regulates degradation by the conjugation of prokaryotic ubiquitin-like protein (Pup) to protein substrates. A rational, structure-based approach was used to design a peptidic inhibitor to target the PafA-Pup interface. Robust inhibition of pupylation was observed both *in vitro* and in cellular lysate, which in conjunction with the proven site-specificity of this interaction, has validated PafA as a druggable target in *M. tuberculosis*. In addition, a proteasome-independent role for pupylation was investigated through ^{1}H NMR spectroscopy studies measuring the rate of the PanB-catalyzed formation of ketopantoate. Pupylation was found to enhance PanB activity suggesting that an increase in the population of Pup-PanB under conditions of stress may also enhance downstream processes responsible for the formation of the waxy cell wall protecting *M. tuberculosis* against the host immune response.

TABLE OF CONTENTS

LIST OF FIGURES

ACKNOWLEDGEMENTS

This thesis would not have been possible without the continuous support of my research advisor, Dr. Champak Chatterjee. Under his guidance, I have not only learned about designing and performing experiments, I have gained a deep appreciation for the dedication and thoughtfulness required to develop meaningful conclusions. I am grateful for the many discussions and for his boundless enthusiasm for science, which was infectious.

I would also like to thank the members of the Chatterjee group, past and present, who kindly donated their time to teach me new lab techniques and were always willing to share their considerable insight. I have learned much during the time I shared with Abhinav Dhall, Ian Eustis, Caroline Weller, Sam Whedon, Patrick Shelton, Alex Santiago, Nick Senger, Christopher Bo, and Dr. Elizabeth Tyson. Additionally, I would like to give a special thank you to Brandon Kier from the Andersen lab for his contributions to my research.

DEDICATION

This thesis is dedicated to my husband, Tim, out of gratitude for his faith and support.

Chapter 1. THE PUP-PROTEASOME SYSTEM IN MTB

1.1 INTRODUCTION

Mycobacterium tuberculosis (Mtb) is the primary causative agent of the infectious disease tuberculosis (TB) and ranks as one of the world's deadliest pathogens. Despite the availability of multiple drugs for over 50 years, TB has remained a threat across the globe, killing 1.5 million people in 2014 alone [1]. A huge challenge in treating and eradicating TB comes from the pathogen's ability to establish a latent, asymptomatic infection within the body, despite a vigorous immune response. Approximately one-third of the world's population has latent TB, and while most are able to suppress its growth, in 5-10% the surviving reservoir of bacteria can be reactivated after years or even decades. Reactivation is widely attributed to a waning immune system, for reasons such as HIV infection, old age and malnutrition, and leads to the progressive disease and active transmission of the pathogen. The mechanisms by which *Mtb* is able to persist within host tissues are not fully understood, however the latent state is characterized by the arrest of progressive cell growth [2]. In contrast, all the conventional anti-TB drugs target processes involved in cell growth and division (Figure 1.1), and while highly effective against actively replicating cells grown *in vitro*, this efficacy is not matched *in vivo* [3]. Treatment of TB is lengthy, requiring a minimum six month course of multiple antibiotics, which can tax the resources of local health care systems, especially in developing countries, and can often be left unfinished. Together, inefficient and incomplete treatment may lead to acquired drug resistance. An estimated 13% of deaths in 2014 were due to multi-drug resistant strains, which are refractory to the two most potent TB drugs, isoniazid and rifampin [4]. 105 countries have reported the emergence of extensively drug-resistant TB, which in addition, will not respond to any fluoroquinolone and at least one of three injectable second-line drugs, amikacin, kanamycin, or capreomycin [5]. The undwindling number of patients left with fewer, less effective treatment options continues to drive an urgent need for a greater understanding of *Mtb* persistence and new therapeutic approaches.

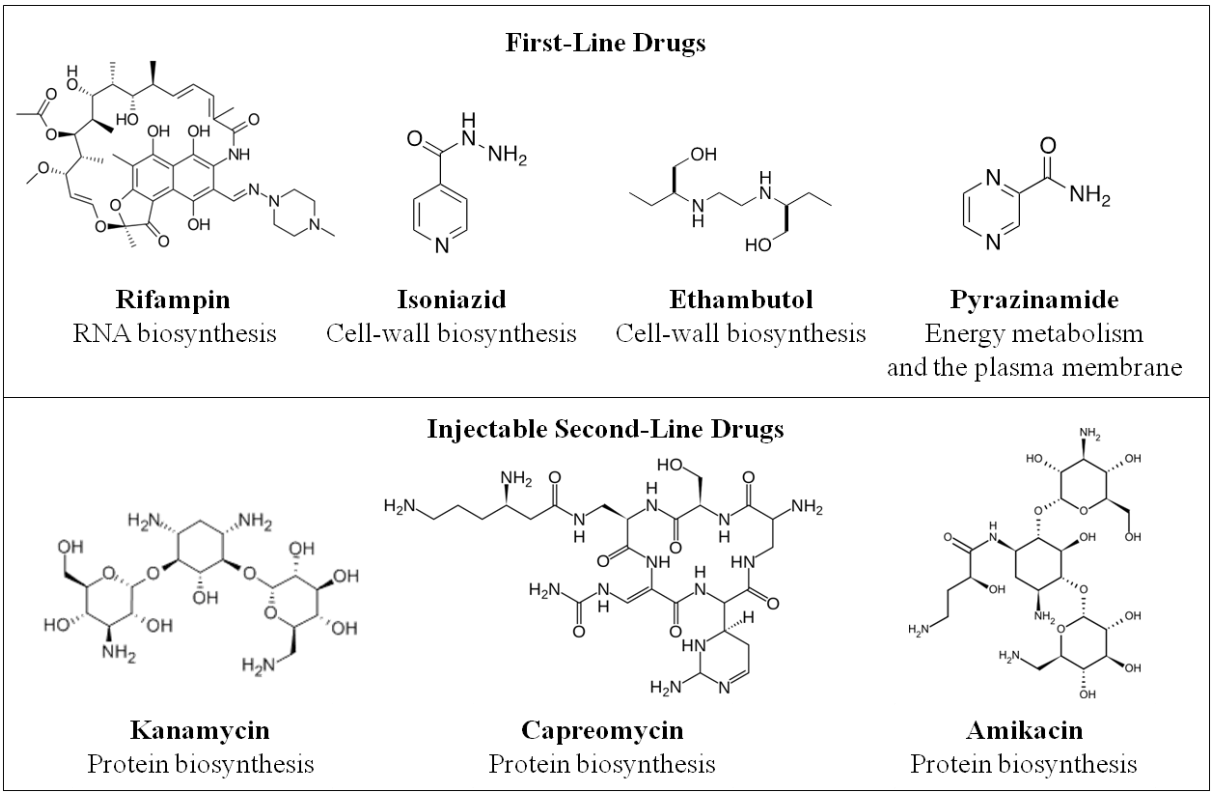

Figure 1.1. Conventional anti-TB drugs target cellular processes of growth and division.

1.2 IMMUNE RESPONSE TO MTB

Mtb is an airborne pathogen, which evades elimination by the host immune response through intracellular persistence in the alveolar macrophage [6]. Inside the macrophage, *Mtb* faces multiple chemical stresses generated to slow the growth of invading pathogens, including a drop in pH, increased toxic ion concentration, and highly reactive oxygen and nitrogen intermediates (ROI and RNI) [7-8]. A pivotal part of the immune response is the expression of inducible nitric oxide synthase (iNOS), which produces the free radical nitric oxide (NO) by the deimination of Arg [9-10]. On its own, NO is neutral and hydrophobic, allowing it to pass cellular and bacterial membranes. However, it has been established that NO can react with sulfhydryl groups in a wide range of essential proteins to regulate their function [11-12] or with the metabolic by-product superoxide to form peroxynitrite, which inflicts oxidative damage on the cell [13-14]. The importance of iNOS has been demonstrated in murine studies; mice lacking a functional iNOS gene ($iNOS^{-/-}$) have been shown to be highly susceptible to *Mtb* infection compared to their wild-type counterparts [15]. Nevertheless, *Mtb* is rarely sterilized even from wild-type mice, which

suggests the pathogen contains defenses to overcome the deleterious effects of NO. It is upon this premise the Pup-Proteasome Pathway was first discovered.

1.3 DISCOVERY OF THE MTB PUP-PROTEASOME PATHWAY

In eukaryotes, the 26S proteasome is composed of two sub-complexes, the 20S core particle and the 19S regulatory cap, which function together to degrade proteins. The 20S core is formed by two pairs of heptameric rings, each made up of α or β subunits, stacked to form a catalytic barrel. The base structure of the 19S regulatory cap includes a hexameric ring of adenosine triphosphatases (ATPases), which serves to recognize, unfold, and translocate substrates into the 20S chamber for degradation [16]. Selectivity for proteolysis is provided through the use of a small, highly conserved protein called ubiquitin, which acts as a tag recognized by the 19S regulatory cap [17]. In *Actinomycetes* like *Mtb*, genes encoding a type of α and β subunit (*prcA* and *prcB*) had previously been identified, but the function and importance of the proteasome was unclear as intracellular proteolysis was known to be carried out by four other proteases of the ClpAP/XP, HslUV, FtsH, and Lon families [18]. In 2003, Darwin et al. [19] were the first to uncover a role of the prokaryotic proteasome by linking it to *Mtb* virulence through resistance to RNI.

Considering the pivotal role of the production of NO to the survival of *Mtb*-infected mice, Darwin et al. performed a genetic screen to identify the *Mtb* genes that confer resistance to RNI. Of the 10,100 transposon mutants screened for hypersensitivity to acidified nitrite, the authors isolated five mutants containing insertions in two genes encoding putative components of the proteasome. One of these genes was named *mpa*, for mycobacterial proteasome ATPase, on the basis of its 82% sequence identity to the first characterized bacterial ATPase, AAA ATPase-forming ring-shaped complex (ARC), of *Rhodococcus erythropolis* [20]. The second gene also had a predicted proteasomal function due in part to its genomic proximity to the *prcBA* genes, and was named *pafA*, for proteasomal accessory factor A. Although *pafA* had no homology to a protein of known function, mutations in both genes produced similar phenotypes *in vitro* and *in vivo*, suggesting that both encode proteins involved in the same pathway. In a similar experiment to the murine study by Nathan and coworkers [15], wild-type and $iNOS^{-/-}$ mice were infected by aerosol with wild-type or *mpa*-mutant *Mtb*. After eight weeks, TB nodules were observable in wild-type mice affected by wild-type Mtb (Figure 1.2A), but were almost completely

consolidated within iNOS$^{-/-}$ mice (Figure 1.2B). In contrast, infection by the *mpa* mutant was highly attenuated (Figure 1.2C). The intermediate pathology observed in iNOS$^{-/-}$ mice (Figure 1.2D), together with a failure of *mpa* and *pafA* mutants to grow in resting primary macrophages, suggests that the disruption of the proteasome pathway sensitizes *Mtb* to more macrophage-associated stresses than those dependent on iNOS.

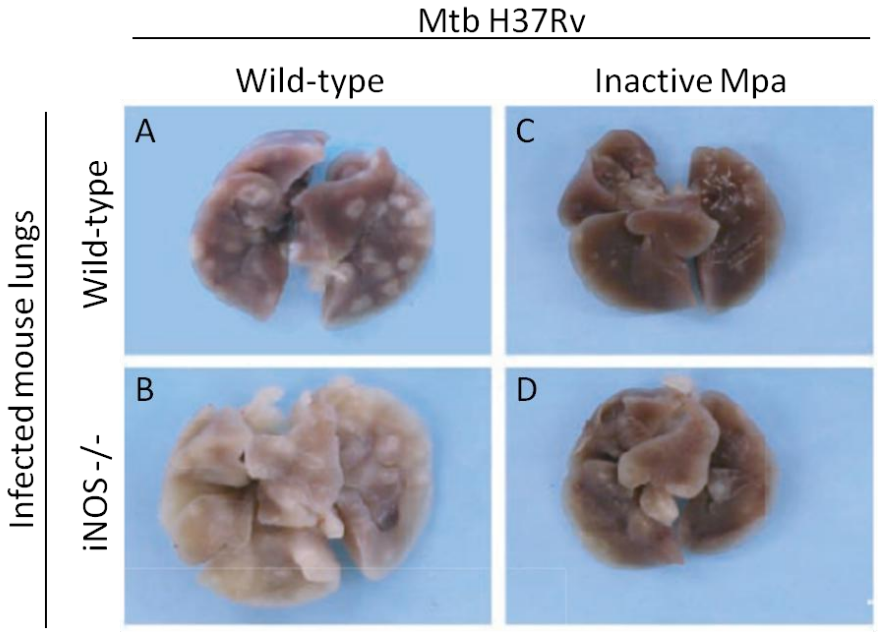

Figure 1.2. Mouse lungs 56 days after infection by aerosol with the *Mtb* strain H37Rv.

From this work it could be concluded that the bacterial proteasome is essential for *Mtb* to resist eradication by NO from host macrophages. However, the biological mechanism for targeting proteins for proteasomal destruction was still unknown, since no sequential homologs of ubiquitin could be found in prokaryotes. The breakthrough in understanding the prokaryotic proteasome came from the identification of prokaryotic ubiquitin-like protein (Pup), a functional homolog of ubiquitin that shares very little sequence identity other than a C-terminal di-glycine motif. Pup was found using an *E. coli* bacterial two-hybrid system with Mpa as the bait [21]. Not only was Pup found to noncovalently interact with Mpa, immunoblot assays with a Pup-specific antibody revealed a ladder of proteins, all targets of the proteasome. Interestingly, the ladder disappeared in a PafA mutant strain of Mtb, suggesting that the interaction between Pup and the protein targets was dependent on PafA and leading to the assignment of PafA as the ligase that covalently attached Pup to proteasome substrates (pupylation) [21].

From these early discoveries, the remainder of Pup-Proteasome Pathway (Figure 1.3) has been pieced together. In many mycobacteria, including *Mtb*, Pup is translated with a C-terminal glutamine, which must be deaminated to a glutamate by the deamidase of Pup (Dop) prior its ligation to the lysine side-chain of a protein substrate [23]. The pupylated substrate can either be degraded by the proteasome or depupylated by Dop [24-25]. Although recent studies have uncovered the mechanism of pupylation and a spectrum of substrates, the ultimate question of how the proteasome system influences *Mtb* virulence has yet to be fully answered.

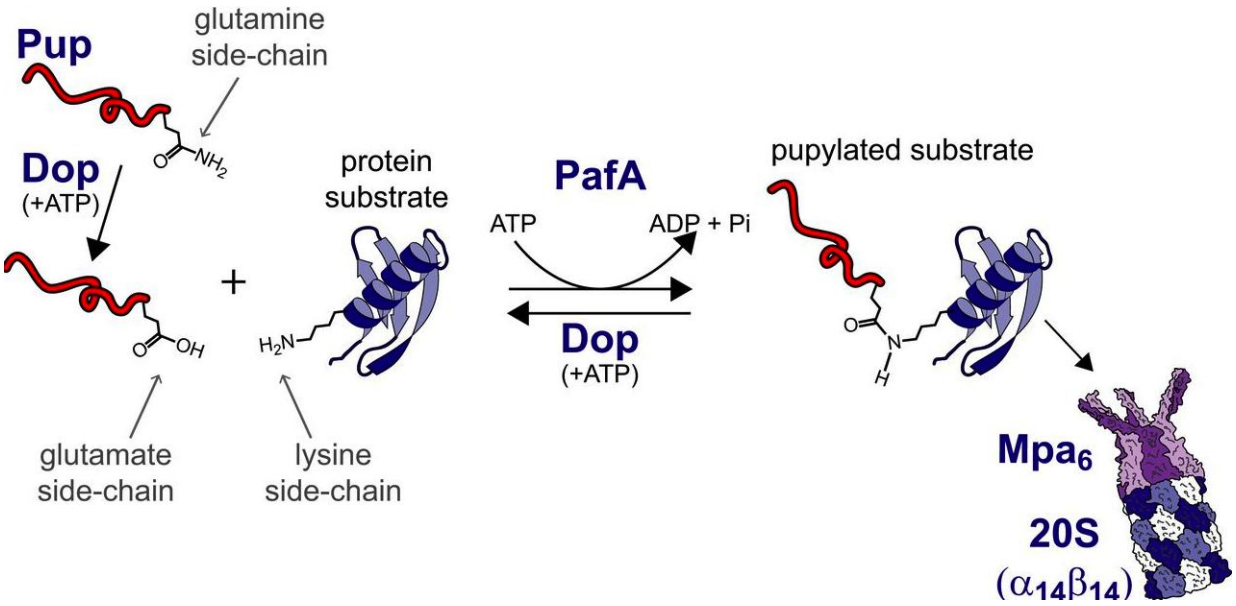

Figure 1.3. The Pup-Proteasome System [22]

1.4 REFERENCES

[1] Tuberculosis Fact Sheet (**2015**) *World Health Organization*, viewed 18 March 2016, <http://www.who.int/mediacentre/factsheets/fs104/en/>

[2] Wayne, L. G.; Sohaskey, C. D. (**2001**) Nonreplicating Persistence of Mycobacterium Tuberculosis, *Annu. Rev. Microbiol.* 55, 139.

[3] McKinney, J. D. (**2000**) In vivo veritas: The search for TB drug targets goes live, *Nature America Inc.* 6, 1330.

[4] Floyd, K.; Raviglione, M. (**2015**) Global Tuberculosis Report 2015, *World Health Organization*.

[5] Tuberculosis Fact Sheet (**2012**) *Centers for Disease Control and Prevention*, viewed 18 March 2016, <http://www.cdc.gov/tb/publications/factsheets/drtb/mdrtb.htm>

[6] Gomez, J. E.; McKinney, J. D. (**2004**) M. tuberculosis persistence, latency, and drug tolerance, *Tuberculosis (Edinb)* 84, 29.

[7] Schnappinger, D.; Ehrt, S.; Voskuil, M. I.; Liu, Y.; Mangan, J. A.; Monahan, I. M.; Dolganov, G.; Efron, B.; Butcher, P. D.; Nathan, C.; *et al.* (**2003**) Transcriptional Adaptation of Mycobacterium tuberculosis within Macrophages: Insights into the Phagosomal Environment, *The Journal of experimental medicine* 198, 693.

[8] Voskuil, M. I.; Schnappinger, D.; Visconti, K. C.; Harrell, M. I.; Dolganov, G. M.; Sherman, D. R.; Schoolnik, G. K. (**2003**) Inhibition of respiration by nitric oxide induces a Mycobacterium tuberculosis dormancy program, *The Journal of experimental medicine* 198,705.

[9] Foster, M. W.; Hess, D. T.; Stamler, J. S. (**2009**) Protein S-nitrosylation in health and disease: a current perspective, *Trends Mol. Med.* 15, 391.

[10] Anand, P.; Stamler, J. S. (**2012**) Enzymatic mechanisms regulating protein S-nitrosylation: implications in health and disease, *J. Mol. Med* 90, 233.

[11] Hess, D. T.; Matsumoto, A.; Kim, S. O.; Marshall, H. E.; Stamler, J. S. (**2005**) Protein S-nitrosylation: purview and parameters, *Nat. Rev. Mol. Cell Biol.* 6, 150.

[12] Hess, D. T.; Stamler, J. S. (**2012**) Regulation by S-nitrosylation of protein post-translational modification, *J. Biol. Chem.* 287, 4411.

[13] Fang, F. C. (**2004**). Antimicrobial reactive oxygen and nitrogen species: concepts and controversies, *Nat Rev Microbiol* 2, 820.

[14] Szabo, C. (**2003**). Multiple pathways of peroxynitrite cytotoxicity, *Toxicol Lett* 140, 105.

[15] MacMicking, J. D.; North, R. J.; LaCourse, R.; Mudgett, J. S.; Shah, S. K.; Nathan, C. F. (**1997**) Identification of Nitric Oxide as a Protective Locus against Tuberculosis, *Proc. Natl. Acad. Sci.* 94, 5243.

[16] Coux, O.; Tanaka, K.; Goldberg, A. L. (**1996**) Structure and functions of the 20S and 26S proteasomes, *Annu. Rev. Biochem* 65, 801.

[17] Glickman, M. H.; Rubin, D. M. Coux, O.; Wefes, I.; Pfeifer, G.; Cjeka, Z. Baumeister, W.; Fried, V. A.; Finley, D. (**1998**) A subcomplex of the proteasome regulatory particle

required for ubiquitin-conjugate degradation and related to the COP9-signalosome and elF3. *Cell* 94, 615.

[18] Butler, S. M.; Festa, R. A.; Pearce, M. J.; Darwin, K. H. (**2006**) Self-compartmentalized bacterial proteases and pathogenesis, *Mol. Microbiol* 60, 553.

[19] Darwin, K. H.; Ehrt, S.; Gutierrez-Ramos, J. C.; Weich, N.; Nathan, C. F. (**2003**) The Proteasome of Mycobacterium tuberculosis is Required for Resistance to Nitric Oxide, *Science* 302, 1963.

[20] Wolf, S.; Nagy, I.; Lupas, A.; Pfeifer, G.; Cejka, Z.; Muller, S. A.; Engel, A.; De Mot, R.; Baumeister, W. (**1998**) Characterization of ARC, a Divergent Member of the AAA ATPase Family from Rhodococcus erythropolis, *J. Mol. Biol.* 277, 13.

[21] Pearce, M. J.; Mintseris, J.; Ferreyra, J.; Gygi, S. P.; Darwin, K. H. (**2008**) Ubiquitin-like protein involved in the proteasome pathway of Mycobacterium tuberculosis, *Science* 322, 1104.

[22] Elharar, Y.; Roth, Z.; Hermelin, I.; Moon, A.; Peretz, G.; Shenkerman, Y.; Vishkautzan, M.; Khalaila, I.; Gur, E. (**2014**) Survival of mycobacteria depends on proteasome-mediated amino acid recycling under nutrient limitation, *EMBO J.* 33, 1802.

[23] Striebel, F.; Imkamp, F.; Sutter, M.; Steiner, M.; Mamedov, A.; Weber-Ban, E. (**2009**) Bacterial ubiquitin-like modifier Pup is deamidated and conjugated to substrates by distinct but homologous enzymes, *Nat. Struct. Mol. Biol.* 16, 647.

[24] Burns, K. E.; Cerda-Maira, F. A.; Wang, T.; Li, H.; Bishai, W. R.; Darwin, K. H. (**2010**) "Depupylation" of prokaryotic ubiquitin-like protein from mycobacterial proteasome substrates, *Mol. Cell* 39, 821.

[25] Imkamp, F.; Striebel, F.; Sutter, M.; Ozcelik, D.; Zimmermann, N.; Sander, P.; Weber-Ban, E. (**2010**) Dop functions as a depupylase in the prokaryotic ubiquitin-like modification pathway, *EMBO Rep.* 11, 791.

Chapter 2. INHIBITION OF THE PUP-PAFA BINDING INTERFACE

2.1 INTRODUCTION

The overarching goal of research on the Pup-Proteasome System is to identify and validate novel druggable targets in *Mtb* that are required for the progression of TB. The strategy presented in this Chapter differs entirely from typical high-throughput small-molecule screening strategies and traditional cationic antimicrobial peptides, as it targets a specific protein-protein interaction that is key to protein degradation in *Mtb*. Strategies to interfere with protein degradation in *Mtb* have continued to target the catalytic activity of the 20S proteasome, but the challenge therein is the mechanistic similarity of eukaryotic and prokaryotic proteasomes [1]. As there are no human analogs of PafA and Pup, the off-target effects of a peptidic inhibitor are anticipated to be minimal when specifically targeting protein pupylation.

In this Chapter, the design of a short peptide, which mimics the hydrophobic and electrostatic interactions in Pup essential for binding to PafA, is discussed. Results are then presented demonstrating the inhibition of pupylation by the synthesized peptide both *in vitro* and in cellular lysate.

2.1.1 *Discovery of key Pup-PafA interactions*

Unlike the well-folded ubiquitin, Pup is disordered in buffered solutions, with no structural motifs seen in circular dichroism (CD) spectra and minimal helicity inferred from NMR experiments [2-4]. Using a series of N-terminally truncated Pup mutants followed by site-directed mutagenesis of conserved hydrophobic residues near the C-terminus, Smirnov et al. identified Pup(39-64) as a minimal ligase recognition motif in *Mtb* Pup [5]. This motif comprises the C-terminal 26 amino acids of Pup, which are highly conserved in a range of disease-causing actinomycetes (Figure 2.1).

```
                                  1                                                  39
M. tuberculosis     ----------MA-------QEQTKRGGGGGDDDDIAGST-AAGQERREKLTEETDDLLDEIDDVLEENAEDFVRAYVQKGGQ 64
C. glutamicum       ----------MN-------AKQTQIMGGGGRDEDNAEDS-AQASGQVQINTEGVDSLLDEIDGLLENNAEEFVRSYVQKGGE 64
M. leprae           ----------MA-------QEQTRR-GGGGDDDEFTSST-SVGQERREKLTEETDDLLDEIDDVLEENAEDFVRAYVQKGGQ 63
C. diphtheriae      ----------MNQN-----GSQIHSGGNGYSDDTDTPGVSSGQS----VNTAGVDDLLDEIDGLLESNAEEFVRSYVQKGGQ 63
T. paurometabola    ----------MA-------QEQTHR-GGGSDDDDLTPDG-GAGQERREKLAEETDDLLDEIDDVLEENAEDFVRAYVQKGGQ 63
G. bronchialis      ----------MA-------QEQTKR-GGGDDDGDLGPEG-GAGQERREKLSEDTDDLLDEIDDVLEENAEDFVRAYVQKGGQ 63
N. farcinica        ----------MA-------QEQTKRTGGGDEDEGSAGPE-AAGQERREKLAEDTDDLLDEIDDVLEENAEDFVRAYVQKGGQ 64
```

Figure 2.1. Sequence alignment of Pup homologues in Actinomycetales.

The sequences of Pup homologues from different actinomycetales strains were aligned with ClustalW. Known pathogens are in red. Residues highlighted in yellow are completely conserved and residues highlighted in pale blue are strongly conserved. Residue numbering is based on the Mtb sequence. Leu39 and Leu40 in Pup, which are important for PafA function, are colored green.

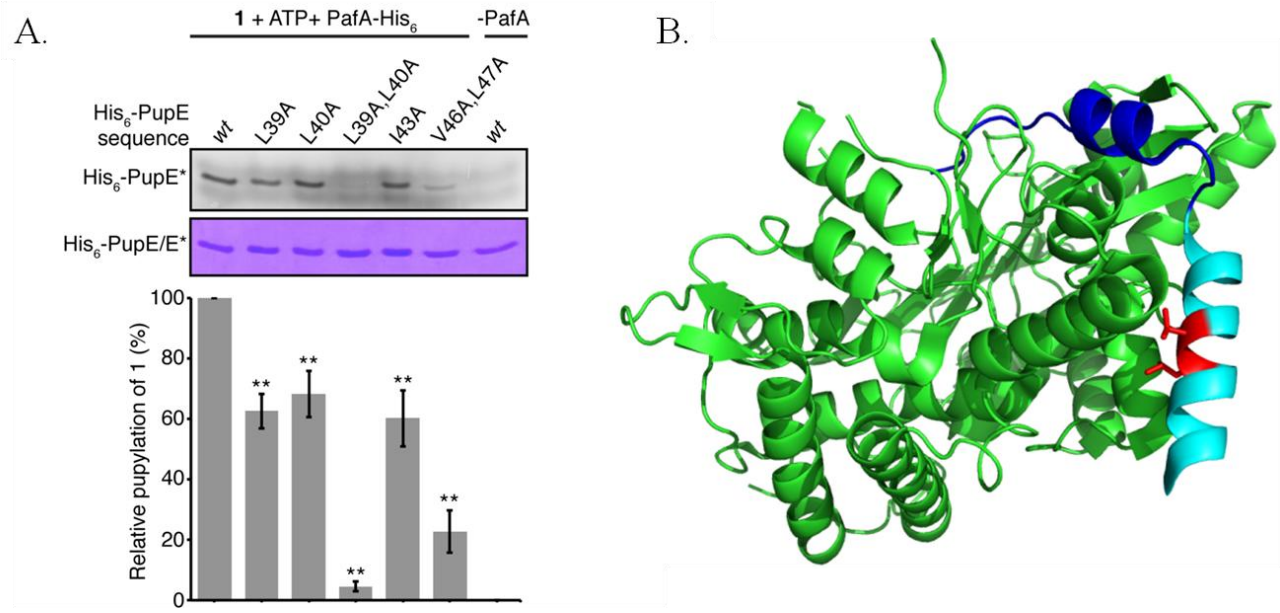

Figure 2.2. Identification of key Pup-PafA interactions.

(A) 15% SDS-PAGE gel of PafA-mediated labeling of His6-PupE polypeptides by fluorescent probe: (top) gel slice showing in-gel fluorescence of labeled proteins; (bottom) Coomassie-stained gel slice as a loading control. The bar graph below shows the quantification of the in-gel fluorescence of each mutant relative to wt Pup after normalization for protein loading. Error bars are standard deviations (n=3). (B) Crystal structure of *Cglu* PafA-Pup(38-64). Leu39/Leu40 side-chains are colored red, N- and C-terminal helices of Pup are colored cyan and blue, respectively. PafA is colored green. PDB code 4BJR

Furthermore, Ala mutagenesis of conserved hydrophobic residues in Pup, specifically Leu39, Leu40, Ile43, Val46 and Leu47, resulted in decreased protein pupylation indicating that they are important for PafA activity (Figure 2.2A) [5]. The most dramatic decrease in pupylation was seen for the Pup(L39A,L40A) double mutant. The importance of Leu39 and Leu40 in the Pup-PafA interaction was further seen from the X-ray structure of a PafA-Pup(40-64) fusion protein from *Corynebacterium glutamicum (Cglu)* [6]. This structure revealed that portions of Pup adopt an α-helical structure when bound to PafA, and that Leu39 and Leu40 make key hydrophobic interactions with PafA (Figure 2.2B). Isothermal titration calorimetry experiments with C-terminally truncated Pup peptides revealed that the N-terminal helix of Pup (cyan in Figure 2.2B), which includes Leu39 and Leu40, contributes ~80% of the binding energy. Based on these observations, it was hypothesized that a short α-helical peptide containing the same conserved hydrophobic and electrostatic interactions as the N-terminal region of Pup could competively bind PafA to inhibit pupylation.

2.1.2 *Trp-cage miniprotein as a helical cap*

The challenge in designing short helical peptides as inhibitors of protein-protein interactions stems from the helix-coil transition theory in peptides [7], which suggests that pre-organization of the first three consecutive residues into a helical turn is energetically demanding and inherently limits the stability of short peptide helices [8-9]. A functional peptide inhibitor would require an additional means of stabilizing the α-helical structure; therefore, a Trp-cage was incorporated into the design.

At 18-20 residues, the Trp-cage is the smallest known miniprotein with tertiary interactions, multiple secondary structure elements, and a hydrophobic core [10]. As a partly α-helical miniprotein with significant aromatic interactions, the extent of folding of Trp-cage variants can be quantitated by circular dichroism (CD) or NMR. The driving force for the folding of the Trp-cage is the total burial of a tryptophan side-chain (Figure 2.3A) [11]. This central Trp residue makes essential contacts with a Tyr and Leu on the same helix. A Gly in the C-cap of the α-helix, a second Trp (or optionally Pro) in the 3-10 loop, an Arg side-chain, and another Pro complete the cage around the central Trp. Additionally, the Trp-cage is stabilized by a helical N-capping Asp residue, a crucial Tyr-Pro interaction, an Arg-Asp salt-bridge, and in some variants, optional entropically favorable Gly to D-Ala replacements. Importantly, residues that make up

the exterior surface of the α-helix do not display important structuring interactions and are largely Ala or Lys, and the Trp-cage α-helix can be N-terminally extended as needed. These extensions, as long as they do not include too many Gly residues, benefit the fold-stability of the miniprotein as a whole. The Trp-cage was envisioned to be a large, but easily accessible, C-terminal capping motif for any α-helix, with a helix-stabilizing effect that is orders of magnitude greater than other known C-terminal caps such as a C-terminal Arg or Schellman loops [12].

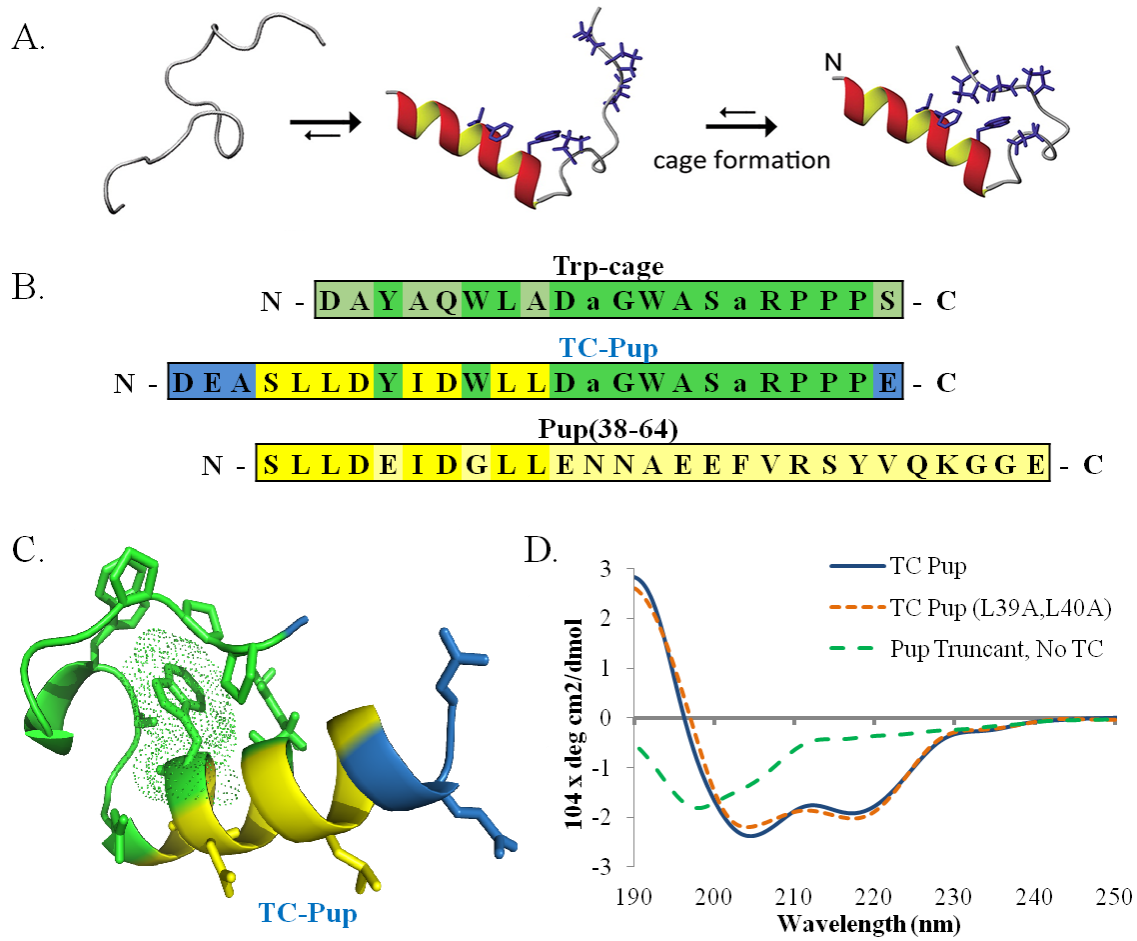

Figure 2.3. Design of a Trp-cage-Pup chimeric peptide (TC-Pup).

(A) Sequences of the original Trp-cage (top), Pup(38-64) (bottom), and the TC-Pup chimeric peptide (middle). Residue colors in TC-Pup indicate the parent sequence. Residues in blue were added for stability. (B) Structure of the Trp-cage mini-protein showing burial of the Trp side-chain (highlighted in mesh) in a hydrophobic cage that includes Pro and Gly residues (green). Residues specific to TC-Pup were grafted onto the Trp-cage structure using PyMol and are colored to match the sequence in A. (C) CD spectra of TC-Pup indicating α-helicity (solid, blue line). Removal of the C-terminal Trp-cage end-cap yields a random coil (dashed, green line). The L39A/L40A mutant of TC-Pup retains its α-helical conformation (dotted, orange line).

It was hypothesized that a short α-helical Pup peptide could be stabilized by grafting its conserved residues on one face of the N-terminal helix of the Trp-cage miniprotein. The rational design of the first Trp-cage-Pup chimeric peptide (TC-Pup) is shown in Figure 2.3B and C. Key design elements in addition to Trp-cage residues included acetylation of the N-terminus to stabilize the helix and reduce unfolding and the addition of a Glu at the C-terminus to increase solubility and provide electrostatic interactions with Arg195 in PafA. Two variations were designed in conjunction with the predicted inhibitor: (1) a Pup truncant, which excludes the last eleven Trp-cage residues (aGWASaRPPPE) to demonstrate the significance of the helical structure to the peptide's inhibitory capability, and (2) a TC-Pup (L39A,L40A) double mutant to demonstrate the site-specific binding of PafA. CD spectra show that the synthetic peptides indeed adopt the expected helical structure, unless the Trp-cage is not present. (Figure 2.3D**)**.

2.2 RESULTS AND DISCUSSION

2.2.1 *Inhibition of protein pupylation in vitro and in cellular lysates*

The effect of the synthesized TC-Pup peptide on protein pupylation by PafA was tested in *in vitro* pupylation assays performed with 10 μM Pup, 1 μM PafA and 10 μM of PanB, one of the first identified substrates of pupylation in *Mtb* [13]. Robust inhibition of protein pupylation was observed in assays with TC-Pup with the degree of inhibition varying in a dose-dependent manner (Figure 2.4A). Dose-response curves were fit by nonlinear regression to the pupylation data (Figure 2.4B) quantified by densitometric analysis of the Pup-PanB band, and the half maximal inhibitory concentration (IC_{50}) was calculated to be 12.84 ± 0.01 μM. Importantly, inhibition depends upon the presence of Leu39/Leu40 analogs in TC-Pup, and the Pup truncant alone does not inhibit pupylation. This exciting result indicated that a short α-helix providing critical interactions found in full-length Pup can inhibit PafA function. An obvious concern when using peptidic inhibitors is their stability to proteolysis in the cellular milieu and their non-specific binding to other proteins. Therefore, TC-Pup was tested in *E. coli* lysate by employing a fluorescent probe, *N*(α)-Fluorescein-5-carboxamide lysine (Nα-5-FAM-L-Lys, or FAM), to follow PafA activity (Figure 2.4C) [4]. Conjugation of Pup with FAM gives a fluorescent Pup band in gels, which is reduced with the inhibition of PafA. Significantly, TC-Pup inhibited PafA activity in lysate (Figure 2.4D).

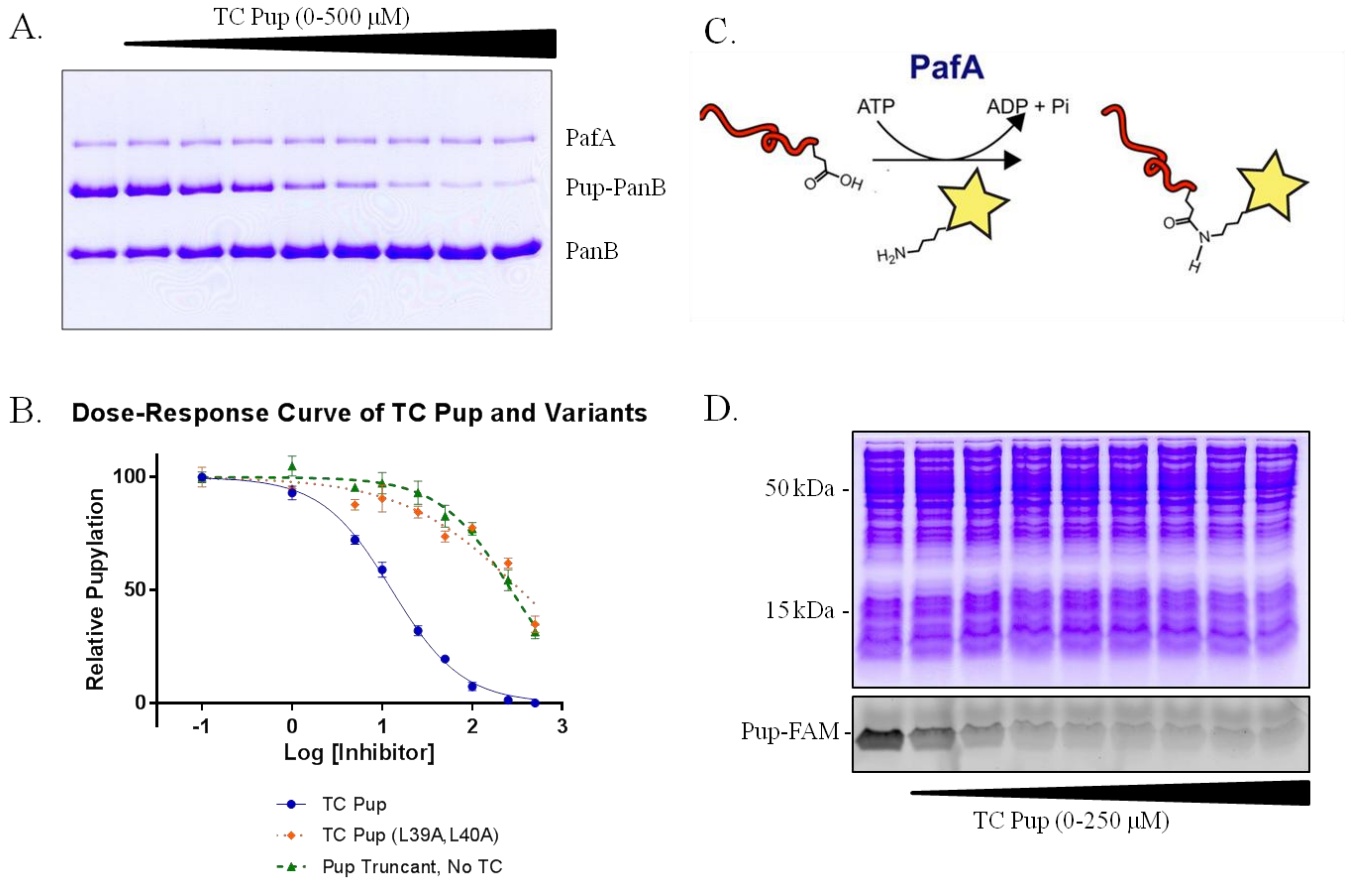

Figure 2.4. Inhibition of protein pupylation *in vitro* and in cellular lysates.

(A) 12% SDS-PAGE gel showing inhibition of PanB pupylation with increasing concentrations of TC-Pup. (B) Quantification of inhibitor potency for the TC-Pup inhibitor and variations thereof. TC-Pup (L39A,L40A) is a mutant of TC-Pup that is missing critical Leu residues. The Pup truncant lacks the Trp-cage residues required for secondary structure. Error bars are standard deviations (n=3). (C) Scheme demonstrating the conjugation of a fluorescent probe to PupE to follow PafA activity. (D) 15% SDS-PAGE gel showing inhibition of pupylation of a fluorescent probe in *E. coli* lysate. The bottom gel slice shows fluorescence arising from Pup-FAM.

2.2.2 *Determination of the affinity constant (K_i)*

To further quantify the potency of TC-Pup, the affinity constant (K_i) was determined using the Cheng-Prusoff relationship (Eqn 2.1) for a reversible, competitive inhibitor [14]. Unlike an IC_{50} value, K_i does not depend on substrate concentration, and is thus a more universal measure of inhibition for the direct comparison of data. The Cheng-Prusoff equation allows the computation of the affinity constant by relating it to the IC_{50} experimentally determined at a fixed substrate concentration, [S].

$$K_i = \frac{IC_{50}}{\left(1 + \frac{[S]}{K_m}\right)} \tag{2.1}$$

This equation requires knowledge of the affinity of the substrate for the enzyme by way of the Michaelis constant (K_m). A Michaelis constant for the PupE-PafA interaction of *Mtb* had previously been reported as 1.4 ± 0.24 μM [15]. Although expected to be similar, since TC-Pup was designed and tested to inhibit the *Cglu* PupE-PafA interaction, the K_m for this pairing was re-determined. *In vitro* pupylation assays designed to maintain steady-conditions was performed using 0.5 μM PafA, 10 μM of PanB, and concentrations of PupE varying from 0.5 – 10 μM. Samples were taken at early time points of 2, 5, and 10 min while the rate of pupylation still proceeded linearly (Figure 2.5A and B). A fit of the Michaelis-Menten saturation curve by nonlinear regression yielded a K_m of 1.14 ± 0.26 μM (Figure 2.5C), similar to the previously reported value for *Mtb*. Using the IC_{50} of 12.84 ± 0.01 μM determined at 10 μM concentration of PupE, a K_i of 1.3 was calculated for the TC-Pup inhibitor.

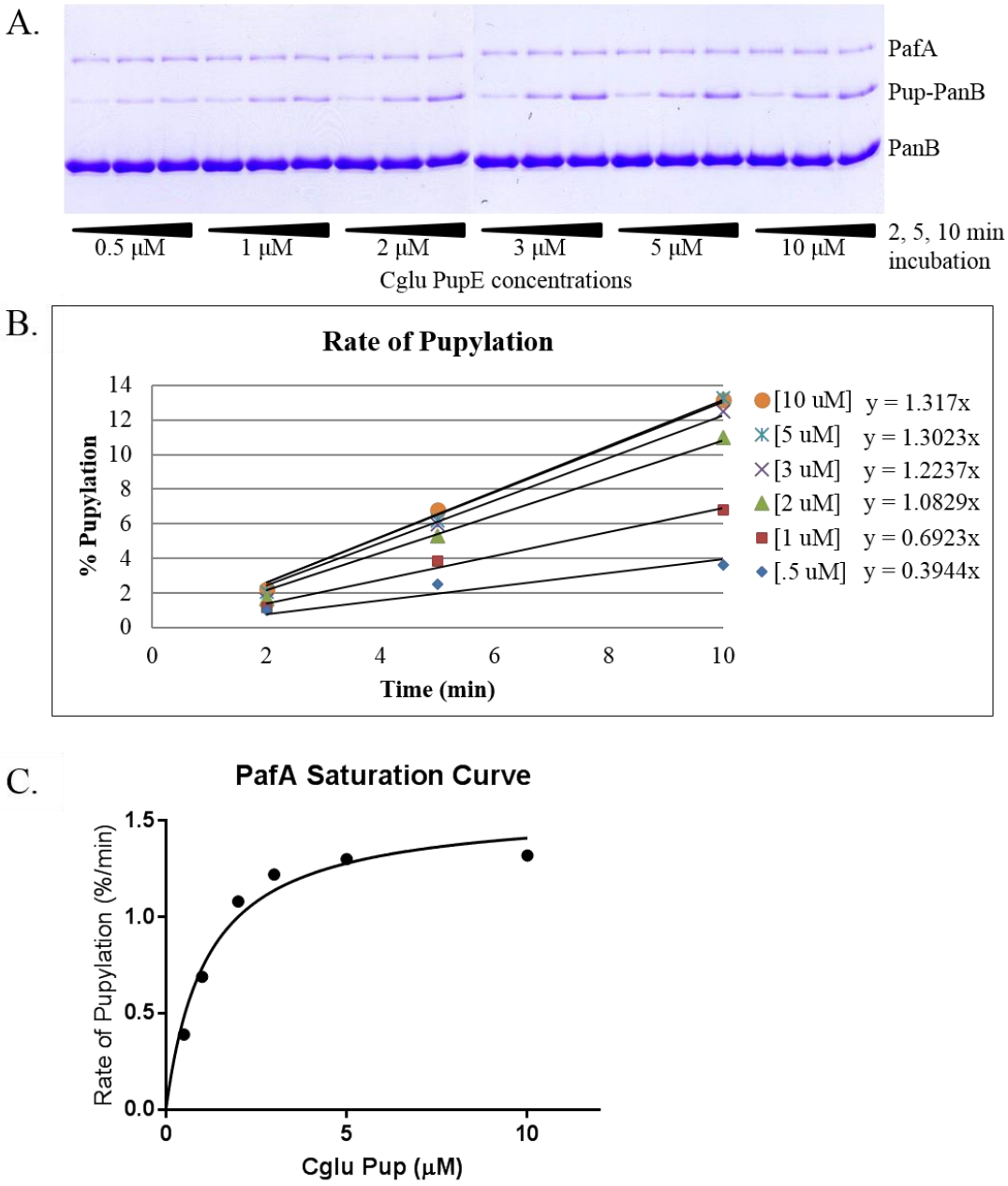

Figure 2.5. Determination of an apparent Michaelis constant for *Cglu* Pup

(A) 12% SDS-PAGE gel showing PanB pupylation for 0.5 – 10 µM concentrations of Pup and 2, 5, and 10 min incubation times. (B) Quantification of pupylation by densitometric analysis after normalization for protein loading to total PanB content (n=3). (C) Michaelis-Menten enzyme saturation curve from the rates of pupylation in B.

2.2.3 *Design modifications to improve inhibition*

With the success of the first rationally designed inhibitor of protein pupylation, several possibilities were considered for improving the inhibitor-PafA interaction to enhance the potency of inhibition. Three changes were made to the original TC-Pup design in order to obtain an improved inhibitor, TC-Pup 2 (Figure 2.6A). First the N-terminus was extended by 3 residues to lengthen the helix and improve its folding [16]. Then an Arg and D-His were introduced in place of Ala and D-Ala, respectively, in order to form additional salt-bridges with PafA. These changes were incorporated simultaneously, as well as individually, and tested at a 15 μM concentration in the *in vitro* pupylation assay in order to obtain a side-by-side comparison of all peptide variations (Figure 2.6B). Indeed, when compared with the original TC-Pup, TC-Pup 2 was shown to be an improved inhibitor of PafA (49.8 ± 1.3% inhibition by TC Pup, 60.1 ± 2.6% inhibition by TC Pup 2, Figure 2.6C). The most significant contribution to inhibitory capability appears to have come from the mutation to Arg, likely due to the formation of a salt-bridge with the proximal Asp25 in PafA, but this change alone does not account for the improved inhibition of TC-Pup 2. This suggests that the TC-Pup-PafA interface can be further optimized.

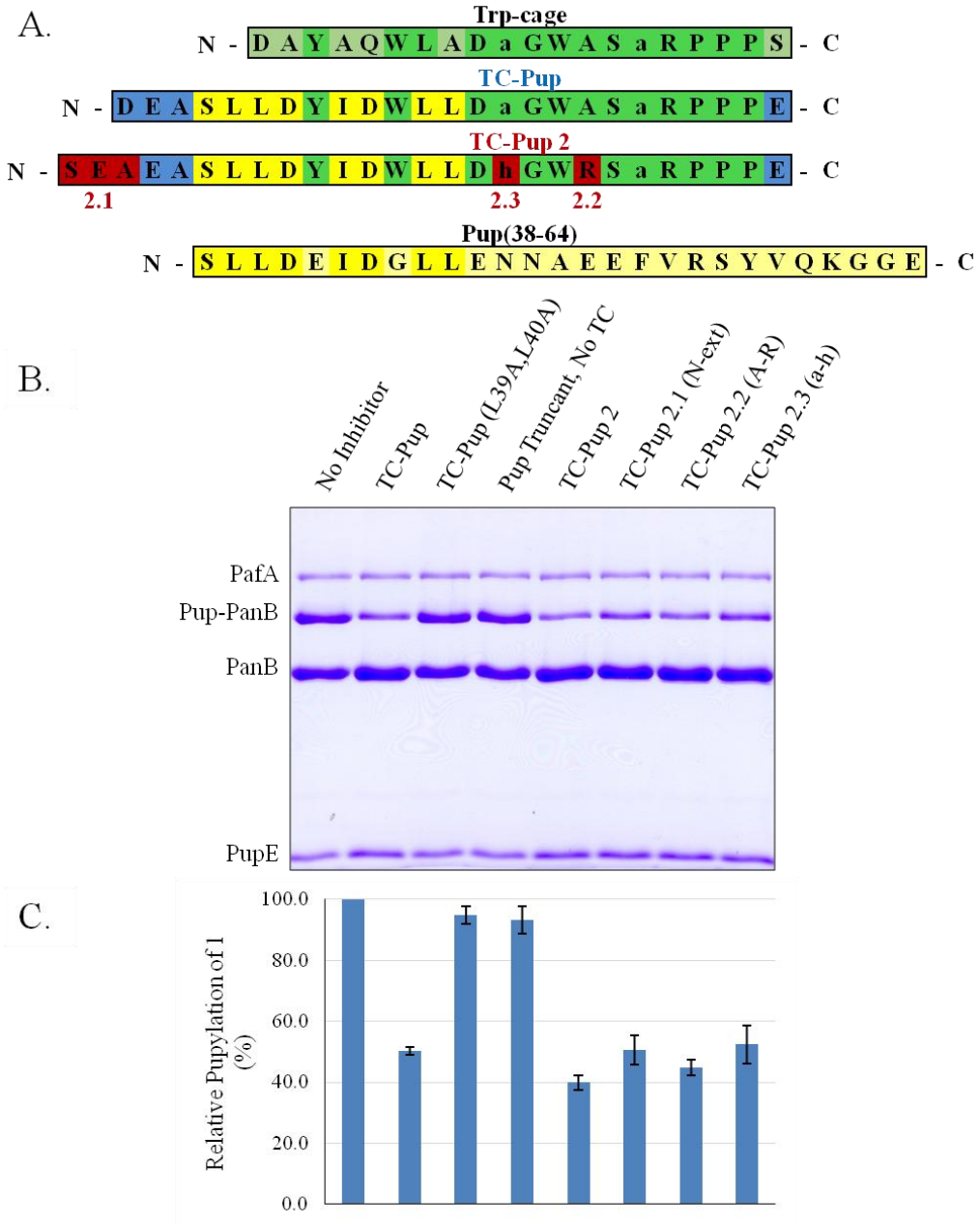

Figure 2.6. Design and analysis of an improved peptide inhibitor, TC-Pup 2.

(A) Sequences of the original Trp-cage (top), Pup(38-64) (bottom), the original TC-Pup (top middle), and TC-Pup 2 (bottom middle). Residues in red indicate a change from TC-Pup to TC-Pup 2. (B) 12% SDS-PAGE gel showing varying degrees of inhibition of PanB pupylation by the first and second-generation inhibitors. With the exception of the far left lane, in which no inhibitor was included, all assays contain 15 μM of the indicated peptide. (C) Bar graph showing the quantification of pupylation relative to the control with no inhibitor after normalization for protein loading. Error bars are standard deviations (n=3).

2.3 CONCLUSION AND OUTLOOK

The TC-Pup chimera provides an excellent platform for initial inhibitor optimization due to its straightforward assembly and well-defined fold. Possible approaches should attempt to maximize the binding interface with PafA and increase the conformational stability of the helical segment of the peptide. The identification of optimal residues at the Pup-PafA helical interface could be accomplished by the standalone Foldit user interface, which employs the Rosetta modeling framework developed at the University of Washington [17]. Foldit allows direct manipulation of peptide side-chains and their conformations, providing energy scores for the final Pup-PafA complex. As another option, with the discovery that the Ala-to-Arg mutation of TC-Pup 2 leads to improved inhibition, this position could be varied with basic residues L- or D-Arg/ Lys/His/Ornithine in order to optimize the salt-bridge formation with Asp25 in PafA. The best analogs would be identified in inhibition assays as before. Finally, the structural and proteolytic stability of the best TC-Pup analog could be enhanced through the cyclization of the peptide by means of a thioether linkage between the N- and C-termini of the inhibitor, or by coupling the C-terminus to a non-essential Lys side-chain. The Andersen lab previously demonstrated that cyclization confers conformational stability to Trp-cage peptides [18]. Stabilization of the TC-Pup conformation would enhance the benefits of an optimized interface with PafA.

At 23-26 amino acids, the size of the TC-Pup scaffold may pose a limitation when faced with penetrating the notoriously waxy *Mtb* cell wall. It is important to note, however, that the successful design of this peptide inhibitor has validated the PafA-Pup interface as a druggable target. In addition, since it is genetically encodable with only slight modifications to the D-Ala residues and functional in live cell cultures, it could provide a powerful and complementary chemical genetic tool to study the effects of inhibiting pupylation at different stages of mycobacterial growth, to include growth under environmental stresses. The advantage of employing an inhibitor that is genetically encodable is that it can be incorporated in the bacterial chromosome by well-established homologous recombination techniques [19] and expressed at different stages of cell growth by using inducible promoters. This is a superior approach to knocking out the PafA gene altogether, as it more closely mimics the effect of therapeutic intervention on growth.

2.4 EXPERIMENTAL PROCEDURES

2.4.1 *General methods*

Nα-5-FAM-L-Lys was purchased from AnaSpec (Fremont, CA). All commonly used chemical reagents and solvents were purchased from Sigma-Aldrich Chemical Company (Milwaukee, WI) or Fischer Scientific (Pittsburgh, PA). Chemically competent DH5α and BL21(DE3), cells were purchased from Novagen (Madison, WI). The pET3a and pET15b vectors were purchased from EMD Millipore (Billerica, MA). Restriction enzymes and T4 DNA ligase were obtained from New England BioLabs (Ipswitch, MA). Primer synthesis and gene sequencing were performed by Integrated DNA Technologies (Coralville, IA) and Genewiz (South Plainfeld, NJ), respectively. Plasmid mini-prep, PCR purification and gel extraction kits were purchased from Qiagen (Valencia, CA). Cells were sonicated using a Sonifier Cell Disruptor, Model W185 from Heat Systems Ultrasonics (Long Island, NY). Sterile filtration units, 0.45 μm pore-size, were purchased from EMD Millipore or Fisher Scientific. Centrifugal filtration units were from Sartorius (Goettingen, Germany) and dialysis was performed with 3.5 kDa MWCO Spectra/Por®6 Dialysis Membrane (Spectrum Laboratories, Inc.). Nickel affinity chromatography was peformed with HisPur^{TM} Ni-NTA resin (Thermo Scientific, Waltham, MA). Size exclusion chromatography was performed on a Superdex 200 16/600 or Superdex 200 10/300 GL size-exclusion column (GE Healthcare) attached to an AKTA FPLC system from GE Healthcare (Waukesha, WI) equipped with a P-920 pump and UPC-900 monitor. SDS-PAGE gels and Tris-HCl running buffers were prepared as per Sambrook and Russell [20]. Protein molecular weight standards were obtained from Bio-Rad (Hercules, CA). Analytical reversed phase HPLC (RP-HPLC) was performed on a Varian ProStar instrument with a Vydac C18 column (5 micron, 4 x 150 mm), employing 0.1% trifluoroacetic acid (TFA) in water (HPLC buffer A), and 90% acetonitrile, 0.1% TFA in water (HPLC buffer B), as the mobile phases. Typical analytical gradients were 0-73% HPLC buffer B over 30 min at a flow rate of 1 mL/min. Preparative scale purifications were conducted on a Vydac C18 (15-20 micron, 50 x 250mm) at a flow rate of 9 mL/min. LC-ESI-MS analysis was conducted on a Bruker Esquire LC-ion trap spectrometer (Billerica, MA) in conjunction with an HP1100 series HPLC (Palo Alto, CA). UV Absorbance measurements were performed on a Nanodrop 2000c Spectrophotometer (Thermo Scientific) for Protein 280 methodology or a Multiskan Spectrum Microplate Spectrophotometer

(Thermo Labsystems) for Bradford assay. Amino acid analysis was undertaken at the UC Davis Proteomics Core Facility. Peptide Synthesis was performed by Brandon Kier from the UW Chemistry Department's Andersen Lab on a CEM Liberty Blue Peptide Synthesis machine. Circular Dichroism was measured on a JASCO J720 Spectropolarimeter. In-gel fluorescence was measured on a GE Typhoon 9000 Gel Imaging Scanner. ImageJ software (http://rsb.info.nih.gov/ij/) was employed to quantify gels. Kinetic data was plotted using GraphPad Prism 6 software.

2.4.2 *Construction of overexpression plasmids*

PafA-His$_6$ The *pafA* gene was obtained by PCR from genomic DNA of *Corynebacterium glutamicum* (ATCC 13032) employing the forward primer 5'-GGGAATTCCCATGGGCAGTA CCGTGGAATCCGCA-3' (*NcoI*) and reverse primer 5'-GCCTACGCCTCGAGCTAATGATG ATGATGATGATGACTGCGATAGCTCTCCGCATG-3' (*XhoI*). PafA was cloned with a C-terminal hexahistidine-tag between the *NcoI* and *XhoI* restriction sites in the pET15b vector. The correct gene sequence was confirmed by DNA sequencing using T7 forward and reverse primers.

His$_6$-PupE The *pupE* gene was obtained from *C. glu* genomic DNA by PCR with the forward primer 5'-GGGAATTCCATATGAACGCAAAGCAAACCCAAATTATGGGT-3' (*NdeI*) and reverse primer 5'-GCCCGCGGATCCCTATTCGCCACCCTTTTGTACATAGGA-3' (*BamHI*). The PCR product was digested with NdeI and BamHI and ligated into a similarly digested pET15b vector.This yielded N-terminally His$_6$-tagged PupE with a thrombin cleavage site between the tag the protein.

PanB-His$_6$ The PanB gene was obtained from *M. tuberculosis* genomic DNA by PCR with the forward primer 5'-GGGAATTCCATATGTCTGAGCAGACTATCTATGGGGCC-3' (*Nde1*) and reverse primer 5'-GCCCGCGGATCCCTAGTGATGATGATGATGATGGAAACTGTGTT CGTCAGCGGGGAATACCCCGC-3' (*BamH1*). PanB was cloned with a C-terminal hexahistidine-tag between the Nde1 and BamH1 restriction sites in the pE3a vector. The correct gene sequence was confirmed by DNA sequencing using T7 forward and reverse primers.

2.4.3 *General method for the expression and purification of proteins*

All proteins were expressed in *E. coli* BL21 (DE3) cells from isopropyl β-D-1-thiogalactopyranoside (IPTG) inducible plasmids. Cells were grown in LB media (25 g/L) with Ampicillin (100 μg/ml) in 3 L baffled-flasks at 37°C until they reached the OD_{600} of 0.5 – 0.7. *Cglu* PafA and *Mtb* PanB protein expression was induced with 0.15 mM IPTG, *Cglu* Pup expression was induced with 0.3 mM IPTG. The induced *Cglu* PafA culture was grown for an additional 20 hours at 16 °C, *Mtb* PanB for 3 hours at 37 °C, and *Cglu* Pup for 5 hours at 25 °C. Cells were harvested by centrifugation at 6000 xg for 20 min at 4 °C, and the cell pellet was resuspended cell lysis buffer consisting of 50mM Tris, 300mM NaCl, 1mM β-mercaptoethanol, 10% (v/v) glycerol, pH 7.5 at 4 °C. Cells were lysed by sonication at a pulsed 40% duty cycle for three to four, 3-minute periods on ice. The insoluble cellular debris was cleared by centrifugation at 13,000x*g* for 30 min, followed by filtration of the supernatant through a 0.45 μm filter under vacuum. The filtrate containing the His_6-tagged protein was loaded by gravity flow over 5-10 mL HisPur^{TM} Ni-NTA resin pre-equilibrated with lysis buffer. The column was washed with ten column volumes each of lysis buffer containing 0mM, 50 mM, and 100mM imidazole. Protein was eluted from the column with lysis buffer at 500 mM imidazole. Protein containing fractions were identified by 12% or 15% SDS-PAGE and combined for further purification.

Ni^{2+}-column eluates containing *Cglu* PafA and *Mtb* PanB were concentrated in 10 kDa and 3 kDa MWCO Vivaspin 20 centrifugal filters, respectively. Concentrated samples were purified by S200 size-exclusion chromatography on a Superdex 200 16/600 size-exclusion column (GE Healthcare) attached to the AKTA FPLC system. The elution buffer contained 50mM Tris, 300mM NaCl, 1mM EDTA, 1mM DTT, and 10% (v/v) glycerol, pH 7.5 at 4 °C. The purity of the resulting peak was assessed by 12% SDS-PAGE, pure samples were concentrated further, and concentration was determined by Bradford protein assay from Thermo Scientific.

Ni^{2+}-column eluate containing *Cglu* Pup was dialyzed into water for three hours using 3.5 kDa dialysis membrane. The eluate volume was then reduced below 10 mL by vacuum centrifuge, and the lyophilized sample was purified by preparative C18 RP-HPLC using a gradient of 35-70% buffer B over 60 min. The identity of the protein was analyzed by ESI-MS. Protein concentration was estimated from Abs_{280} measurements using a calculated extinction

coefficient (ε) of 1490 M^{-1} cm^{-1} (ExPASy ProtParam) and verified by amino acid analysis undertaken at the UC Davis Proteomics Core Facility.

2.4.4 *General procedure for dose-response and time-point assays*

Pupylation assays were undertaken with 100 μM ATP, 10 μM *Cglu* PupE, 10 μM *Mtb* PanB, 1 μM *Cglu* PafA, and 0, 1, 5, 10, 25, 50, 100, 250, and 500 μM of inhibitor in a 10 μL volume for dose-response assays or 35 μL volume for time-point assays. The reaction buffer consisted of 50 mM Tris-Cl, 300 mM NaCl, 1 mM DTT, 20 mM $MgCl_2$, and 10% (v/v) glycerol at pH 7.6. The reactions were initiated by the addition of PafA, allowed to proceed at 25 °C for 1 hour for the dose-response assays, and quenched by the addition of 6x SDS gel-loading buffer. For the time-point assays, 10 μL aliquots were removed at 1 hr, 2 hrs, and 3 hrs and quenched with gel-loading buffer. Assay products were analyzed by resolving on 12% SDS-PAGE and stainin in Coomassie Brilliant Blue. Pupylation was visualized by the motility shift of PanB when conjugated to PupE over the course of the reaction. A percentage of pupylation was determined by densitometric analysis of the Pup-PanB band relative to the sum of both PanB bands using ImageJ software. Dose-response curves were calculated by nonlinear regression using four-parameter variable slope in GraphPad Prism 6.

2.4.5 *General procedure for assays with cellular lysates*

E. coli BL21 (DE3) cells were grown at 37 °C until they reached an OD_{600} greater than one. The cells were harvested, resuspended in cell lysis buffer, and lysed by sonication. The insoluble cellular debris was cleared by centrifugation at 13,000x*g* for 30 min, followed by filtration of the supernatant through a 0.45 μm filter. The lysate was demonstrated to have no observable PafA activity by conducting a pupylation assay with 500 μM ATP, 100 μM FAM-K, 3 μL lysate containing *Cglu* PupE (taken prior to Ni^{2+}-affinity purification), and 2 μL *E. coli* lysate in a 15 μL total volume for 2 hours at 37 °C. A positive control was undertaken with 2 μL lysate contain *Cglu* PafA (taken prior to Ni^{2+}-affinity purification) in place of the *E. coli* lysate. Fluorescence was imaged as described below. A band corresponding to pup-FAM conjugate was observed in the positive control, but not in the assay containing the newly collected *E. coli* lysate, thus it was determined this lysate could be used in dose-response assays without influencing the rate of pupylation.

Pupylation assays were undertaken with 100 μM ATP, 10 μM *Cglu* PupE, 200 μM FAM-K, 2 μL *E. coli* lysate, 1 μM *Cglu* PafA, and 0, 1, 5, 10, 25, 50, 100, 250, and 500 μM of each inhibitor in a 10 μL volume. The reaction buffer consisted of 50 mM Tris, 300 mM NaCl, 1 mM DTT, 20 mM $MgCl_2$, and 10% (v/v) glycerol at pH 7.6. The reactions were initiated by the addition of PafA, allowed to proceed at 25 °C for 1 hour, and quenched by the addition of 6x SDS gel-loading buffer. Assay products were analyzed by resolving on 15% SDS-PAGE. Fluorescent gels were gently nutated in 45% methanol/10% acetic acid for 10 min to remove unconjugated probes from the gel prior to imaging. The PupE-fluorophore conjugate was subsequently observed by in-gel fluorescence emission at 521 nm using a Typhoon FLA 9000 scanner (GE Healthcare). Following fluorescence imaging, the gels were stained in Coomassie Brilliant Blue to quantify protein loading. Pupylation was determined by densitometric analysis of the Pup-FAM using ImageJ software and calculated as a percentage relative to the assay without inhibitor.

2.4.6 *General procedure for assay to determine K_M of Cglu PupE*

Pupylation assays were undertaken with 0.5, 1, 2, 3, 5, and 10 μM *Cglu* PupE in the presence of 100 μM ATP, 10 μM *Mtb* PanB, and 0.5 μM *Cglu* PafA, in a 35 μL volume at 25 °C. The reaction buffer consisted of 50 mM Tris, 300 mM NaCl, 1 mM DTT, 20 mM $MgCl_2$, and 10% (v/v) glycerol at pH 7.6. The reactions were initiated by the addition of PafA and 10 μL aliquots were removed at 2 min, 5 min, and 10 min and quenched by the addition of 4 μL of 6x SDS gel-loading buffer. Assay products were analyzed by resolving on 12% SDS-PAGE and staining in Coomassie Brilliant Blue. Pupylation was visualized by the motility shift of PanB when conjugated to PupE over the course of the reaction. A percentage of pupylation was determined by densitometric analysis of the Pup-PanB band relative to the sum of both PanB bands using ImageJ software.

2.5 REFERENCES

[1] Lin, G.; Li, D.; de Carvalho, L. P. S.; Deng, H.; Tao, H.; Vogt, G.; Wu, K.; Schneider, J.; Chidawanyika, T.; Warren, J. D.; Li, H.; Nathan, C. (**2009**) Inhibitors selective for mycobacterial versus human proteasomes, *Nature* 461, 621.

[2] Chen, X.; Solomon, W. C.; Kang, Y.; Cerda-Maira, F.; Darwin, K. H.; Walters, K. J. (**2009**) Prokaryotic ubiquitin-like protein pup is intrinsically disordered, *J. Mol. Biol.* 392, 208.

[3] Sutter, M.; Striebel, F.; Damberger, F. F.; Allain, F. H.-T.; Weber-Ban, E. (**2009**) A distinct structural region of the prokaryotic ubiquitin-like protein (Pup) is recognized by the N-terminal domain of the proteasomal ATPase Mpa, *FEBS Lett.* 583, 3151.

[4] Liao, S.; Shang, Q.; Zhang, X.; Zhang, J.; Xu, C.; Tu, X. (**2009**) Pup, a prokaryotic ubiquitin-like protein, is an intrinsically disordered protein, *Biochem. J.* 422, 207.

[5] Smirnov, D.; Dhall, A.; Sivanesam, K.; Sharar, R. J.; Chatterjee, C. (**2013**) Fluorescent probes reveal a minimal ligase recognition motif in the prokaryotic ubiquitin-like protein from Mycobacterium tuberculosis, *J. Am. Chem. Soc.* 135, 2887.

[6] Barandun, J.; Delley, C. L.; Ban, N.; Weber-Ban, E. (**2013**) Crystal structure of the complex between prokaryotic ubiquitin-like protein and its ligase PafA, *J. Am. Chem. Soc.* 135, 6794.

[7] Zimm, B. H.; Bragg, J. K. (**1959**) Theory of the Phase Transition between Helix and Random Coil in Polypeptide Chains, *J. Chem. Phys.* 31, 526.

[8] Henchey, L. K.; Jochim, A. L.; Arora, P. S. (**2008**) Contemporary strategies for the stabilization of peptides in the alpha-helical conformation, *Curr. Op. Chem. Biol.* 12, 692.

[9] Patgiri, A.; Jochim, A. L.; Arora, P. S. (**2008**) A hydrogen bond surrogate approach for stabilization of short peptide sequences in alpha-helical conformation, *Acc. Chem. Res.* 41, 1289.

[10] Neidigh, J. W.; Fesinmeyer, R. M.; Andersen, N. H. (**2002**) Designing a 20-residue protein, *Nat. Struct. Biol.* 9, 425.

[11] Mok, K. H.; Kuhn, L. T.; Goez, M.; Day, I. J.; Lin, J. C.; Andersen, N. H.; Hore, P. J. (**2007**) A pre-existing hydrophobic collapse in the unfolded state of an ultrafast folding protein, *Nature* 447, 106.

[12] Kallenbach, N. R.; Gong, Y. (**1999**) C-terminal capping motifs in model helical peptides, *Bioorg. Med. Chem.* 7, 143.

[13] Pearce, M. J.; Mintseris, J.; Ferreyra, J.; Gygi, S. P.; Darwin, K. H. (**2008**) Ubiquitin-like protein involved in the proteasome pathway of Mycobacterium tuberculosis, *Science* 322, 1104.

[14] Cheng, Y.; Prusoff, W. H. (**1973**) Relationship between the inhibition constant (Ki) and the concentration of inhibitor which causes 50 percent inhibition (I50) of an enzymatic reaction, *Biochem. Pharmacol.* 22, 3099.

[15] Guth, E.; Thommen, M.; Weber-Ban, E. (**2011**) Mycobacterial ubiquitin-like protein ligase PafA follows a two-step reaction pathway with a phosphorylated pup intermediate, *J. Biol. Chem.* 286, 4412.

[16] Barua, B.; Lin, J. C.; Williams, V. D.; Kummler, P.; Neidigh, J. W.; Andersen, N. H. (**2008**) The Trp-cage: optimizing the stability of a globular miniprotein, *Protein Eng. Des. Sel.* 21, 171.

[17] Cooper, S.; Khatib, F.; Treuille, A.; Barbero, J.; Lee, J.; Beenen, M.; Leaver-Fay, A.; Baker, D.; Popovic, Z.; Players, F. (**2010**) Predicting protein structures with a multiplayer online game, *Nature* 466, 756

[18] Scian, M.; Lin, J. C.; Le Trong, I.; Makhatadze, G. I.; Stenkamp, R. E.; Andersen, N. H. (**2012**) Crystal and NMR structures of a Trp-cage mini-protein benchmark for computational fold prediction, *Proc. Natl. Acad. Sci. U.S.A.* 109, 12521.

[19] Husson, R. N. (**1998**) Homologous recombination in Mycobacterium smegmatis. Screening methods for detection of gene replacement, *Methods Mol. Biol.* 101, 199.

[20] Sambrook, D. W.; Russell, J. (**2001**) Molecular Cloning: a laboratory manual, Third Edition**,** *Cold Spring Harbour Laboratory Press*, Cold Spring Harbour, New York 2100.

Chapter 3. EFFECT OF PUPYLATION ON ENZYME ACTIVITY

3.1 INTRODUCTION

Darwin and co-workers recently demonstrated that a key role for pupylation in *Mtb* is to facilitate degradation of the mycobacterial homolog of the plant hormone LONELY GUY (Log) [1]. The normal function of Log is to synthesize cytokinins, which typically break down to give several toxic compounds. One such compound is para-hydroxybenzaldehyde (pHBA), which is lethal to Mtb under nitrosative stress. Therefore, by limiting cellular concentrations of Log, pupylation prevents the toxic accumulation of pHBA and facilitates *Mtb* survival in the host.

It is possible that pupylation directly influences other biosynthetic pathways in *Mtb* that are critical for its ability to survive nitrosative stress. In this regard, it is surprising that a commonly employed model substrate for *in vitro* pupylation studies, the enzyme ketopantoate hydroxymethyltransferase (PanB) that catalyzes the first committed step of pantothenate biosynthesis (Figure 3.1), is pupylated in growing *Mtb* [2]. Pantothenic acid is the key precursor to the essential cofactor, Coenzyme A (CoA), which provides the phosphopantetheinyl linker of the acyl carrier protein (ACP). The PanB catalyzed reaction is known to be the rate-limiting reaction in pantothenate biosynthesis [3]. It was hypothesized that Pup-mediated degradation of PanB may reduce the amounts of CoA and ACP produced, which would have disastrous consequences on mycolic acid biosynthesis. *Mtb* depends upon these long-chain fatty acids for its waxy cell wall that allows it to hide from its host's immune response [4].

In this Chapter, the role of pupylation on the kinetics of PanB action is investigated. Results from ^{1}H NMR spectroscopy studies used to measure both substrate depletion and product formation in the reaction catalyzed by PanB are presented with a comparison of pupylated and unpupylated populations.

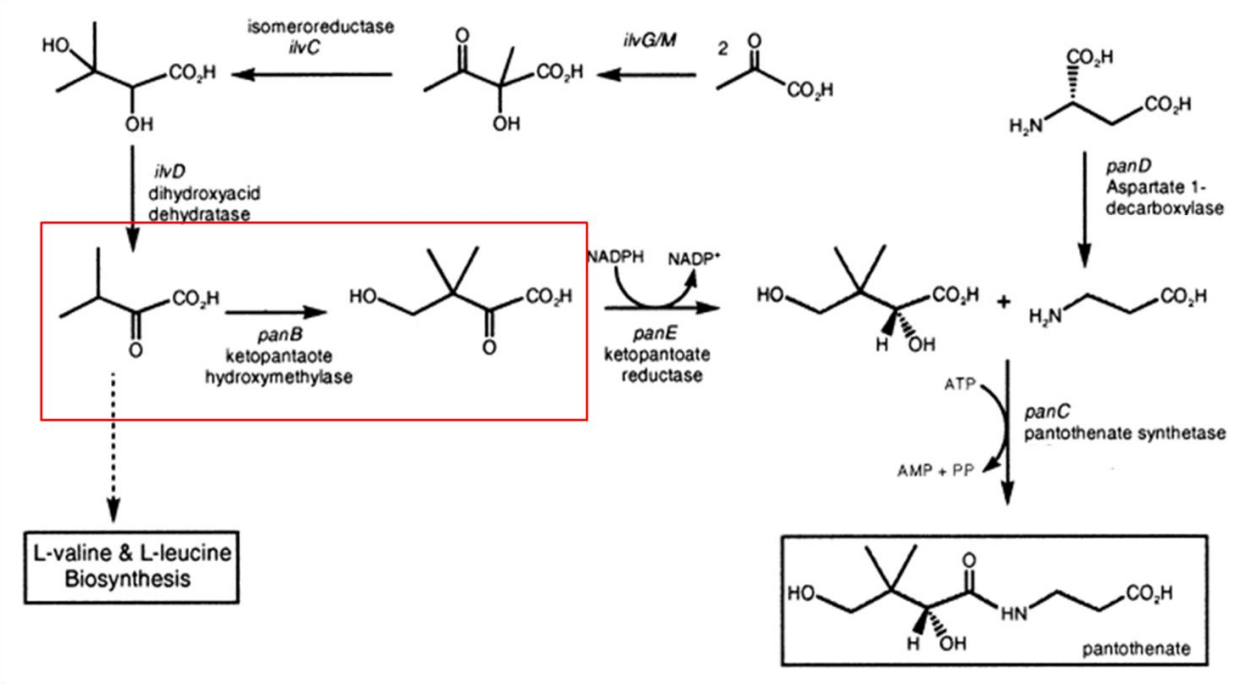

Figure 3.1. Pantothenate biosynthesis in bacteria, plants, and yeast. The box in red shows the conversion of α-ketoisovalerate (α-KIV) to ketopantoate in a reaction catalyzed by PanB [3].

3.2 Results and Discussion

Pupylated PanB was generated by *in vitro* pupylation of purified PanB with Strep-tagged Pup and PafA. This allowed enrichment of the Pup-PanB species to about 94% of the total PanB. Since PanB exists as a dodecamer in solution, purification of Pup-PanB to homogeneity was not possible. Therefore, the Pup-PanB:PanB (94:6) mixture was directly used in ^{1}H NMR assays of PanB activity. Careful consideration was taken to ensure the population of unpupylated PanB was treated in the same manner as the pupylated population, so that any difference in observed catalytic activity could be isolated to the presence of Pup, not differences in the purification process.

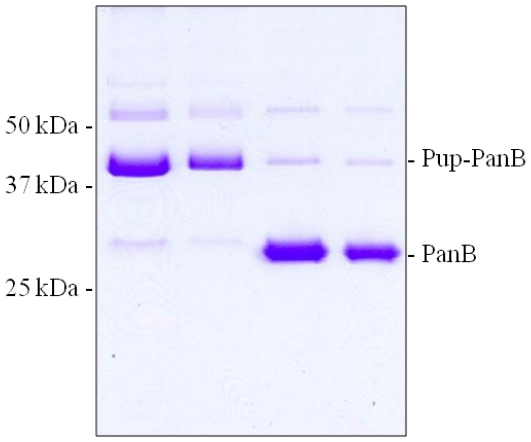

Figure 3.2. Purified enzyme. 12% SDS-PAGE showing purified Pup-PanB:PanB (94:6) and purified PanB:Pup-PanB (6:94).

PanB catalyzes the conversion α-ketoisovalerate (α-KIV) to ketopantoate in a three-step aldol reaction. The first step is the enolization of α-KIV and is followed by the enolate collapse and nucleophilic attack of the methylene group of N_5,N_{10}-methylenetetrahydrofolate (MTHF). A subsequent hydrolysis cleaves the product, ketopantoate, from the cofactor, tetrahyrofolate (THF). The chemical mechanism, as proposed by Sugantino et al. [3], is shown in Figure 3.3.

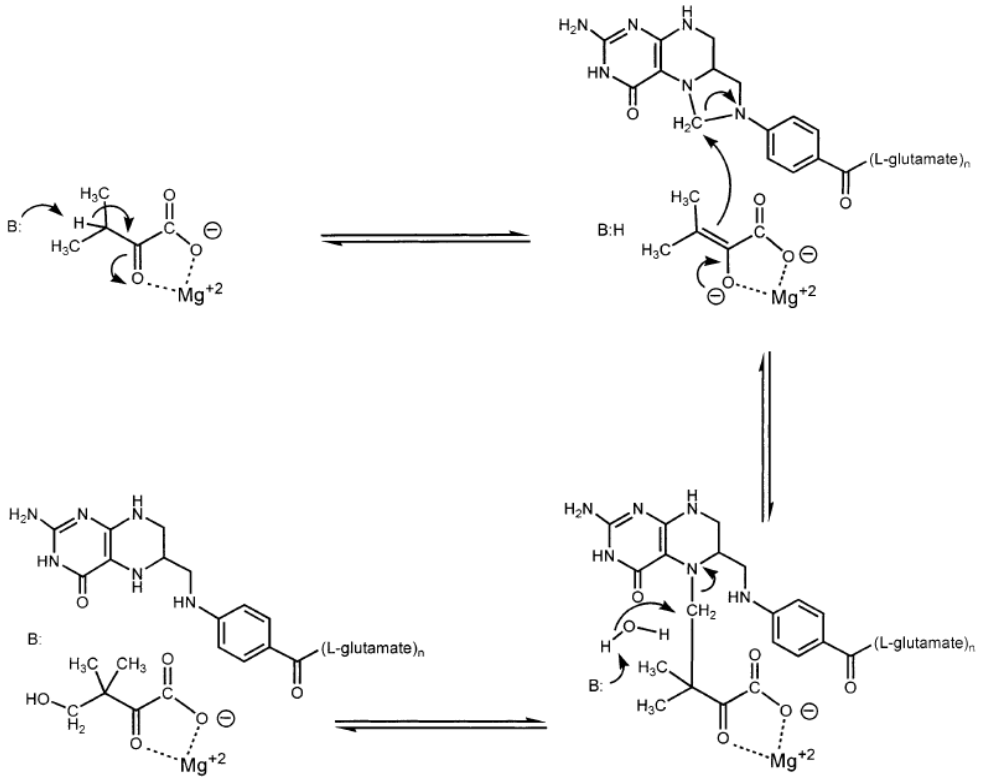

Figure 3.3. Proposed chemical mechanism for hydroxymethyl transfer from N_5,N_{10}-methylenetetrahydrofolate (MTHF) to α-ketoisovalerate (α-KIV) by *Mtb* PanB.

3.2.1 *Enolization of α-KIV*

The first step in the aldol reaction, the formation of the enolate species from α-KIV (Figure 3.4A), was readily seen in ^{1}H NMR studies by the disappearance of the septet arising from the methine proton when the substrate is mixed with PanB in D_2O. The time-course of disappearance of the septet was measured and quantified (Figure 3.4B and C) to identify the effect of pupylation on PanB activity. Surprisingly, Pup-PanB undertakes enolization of α-KIV more than two-fold faster than PanB (k_{enol} PanB = 136 ± 12 min^{-1} vs. k_{enol} Pup-PanB = 300 ± 22 min^{-1}, n= 4), and this rate difference is split in a population in which 50% of PanB is pupylated (k_{enol} 50:50 Pup-

PanB:PanB = 205 min^{-1}, n=1). This unexpected observation suggests that increasing the population of Pup-PanB under conditions of stress may enhance the rate of CoA and ACP formation, which in turn favors mycolic acid biosynthesis.

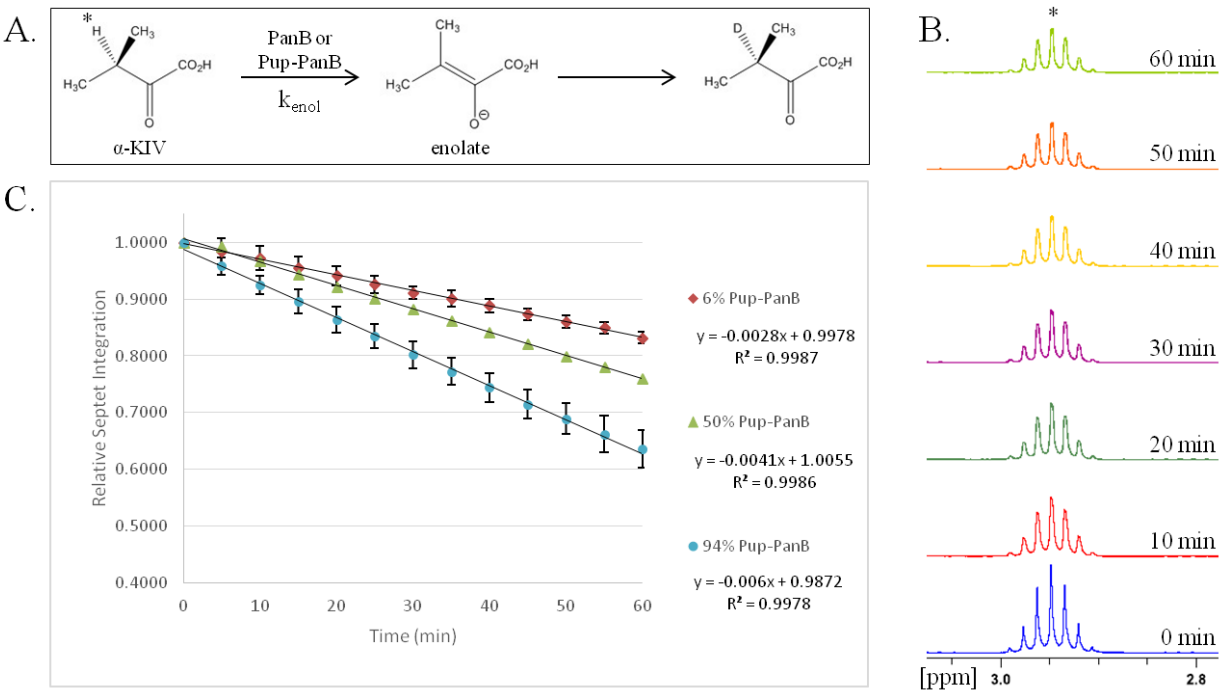

Figure 3.4. Effect of pupylation on PanB-catalyzed enolization of α-KIV.

A.The enolization reaction observed by 1H NMR spectroscopy. B. Overlaid spectra showing the disappearance of the β-proton (marked with an asterisk). C. Plot of the initial, linear rate of activity demonstrating the difference between a 94% PanB population (red diamond), 50% PanB and Pup-PanB population (green triangle), and a 94% Pup-PanB population (blue circle).

3.2.2 *Ketopantoate formation*

The next step was to look at the effect of pupylation on the full aldol reaction catalyzed by PanB. It was possible that the rate enhancement in enolization observed with Pup-PanB may have been negated by poor binding of the co-factor tetrahydrofolate, in which case there would have been no difference in the observed rate of ketopantoate formation. Instead of monitoring the disappearance of reactant α-KIV, the aldol reaction was detected by the formation of product through the appearance of the methyl groups or C4 hydrogen of ketopantoate (Figure 3.5A and B). *In vivo*, the hydoxymethyl group of ketopantoate is obtain from the methylene group of MTHF followed by hydrolysis; however, the aldol reaction can proceed to completion in a THF-

independent manner, through a direct nucleophilic attack of formaldehyde by the enolate. Experimentation revealed that the two-fold rate enhancement was maintained in the THF-independent reaction, (k_{aldol} PanB = 85 min^{-1} vs. k_{aldol} Pup-PanB = 155 min^{-1}). While not quite two-fold, the difference also persisted throughout the aldol reaction in the presence of THF (k_{aldol} PanB = 550 min^{-1} vs. k_{aldol} Pup-PanB = 690 min^{-1}) (Figure 3.5C).

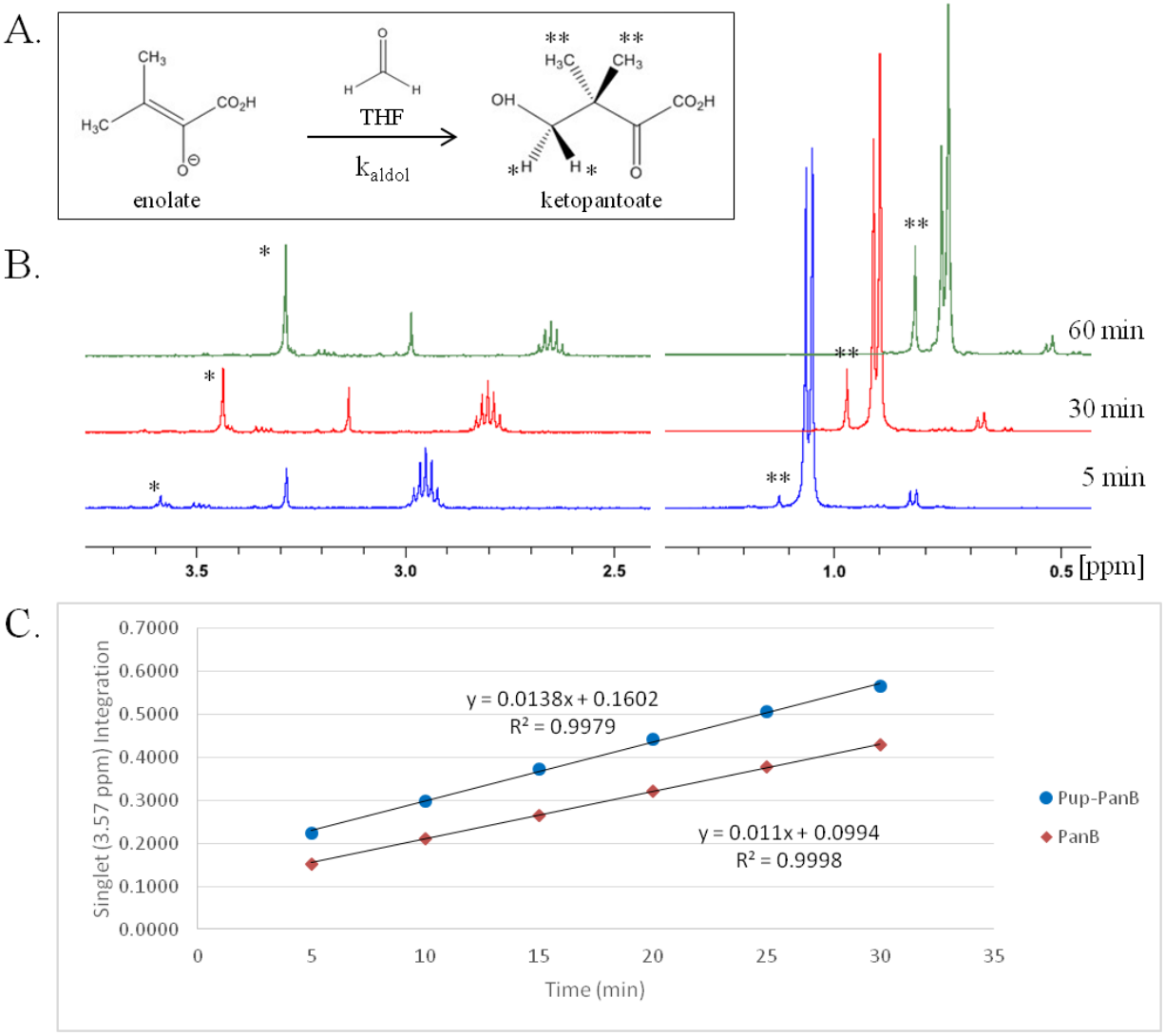

Figure 3.5. Effect of pupylation on PanB-catalyzed ketopantoate formation.

A.The formation of ketopantoate observed by ^{1}H NMR spectroscopy. B. Overlaid spectra showing the appearance of the C4 hydrogens (marked with an asterisk) and rearrangement of the methyl groups (marked with two asterisks). C. Plot of the initial, linear rate of activity demonstrating the difference between a 94% PanB population (red diamond) and a 94% Pup-PanB population (blue circle).

3.3 Conclusion and Outlook

Although previous studies have shown that pupylation of the ATPase, Mpa, renders it functionally inactive [5], the results presented in this Chapter represent the first example of pupylation activating an enzyme. It would be beneficial to corroborate the results by identifying which lysine side-chain of PanB is modified by Pup. The structural implications of a long protein tag on the body of PanB could provide insight to the changes in the active site that may account the differences in activity. The *in vitro* studies could also be expanded to ^{14}C-acetate feeding experiments in growing cultures of *Msm* in the presence or absence of the pupylation inhibitors developed in Chapter 2 [6]. The translation of enhanced pantothenate production to downstream processes would shed light on the role for Pup in the primary metabolism of *Mtb* and its effect on cell-wall biosynthesis.

3.4 Experimental Procedures

3.4.1 *General methods*

All commonly used chemical reagents and solvents were purchased from Sigma-Aldrich Chemical Company (Milwaukee, WI) or Fischer Scientific (Pittsburgh, PA). Chemically competent DH5α and BL21(DE3), cells were purchased from Novagen (Madison, WI). The pET3a and pET15b vectors were purchased from EMD Millipore (Billerica, MA). Restriction enzymes and T4 DNA ligase were obtained from New England BioLabs (Ipswitch, MA). Primer synthesis and gene sequencing were performed by Integrated DNA Technologies (Coralville, IA) and Genewiz (South Plainfeld, NJ), respectively. Plasmid mini-prep, PCR purification and gel extraction kits were purchased from Qiagen (Valencia, CA). Cells were sonicated using a Sonifier Cell Disruptor, Model W185 from Heat Systems Ultrasonics (Long Island, NY). Sterile filtration units, 0.45 μm pore-size, were purchased from EMD Millipore or Fisher Scientific. Centrifugal filtration units were from Sartorius (Goettingen, Germany), and dialysis was performed with 3.5 kDa MWCO Spectra/Por®6 Dialysis Membrane (Spectrum Laboratories, Inc.). Nickel affinity chromatography was performed with HisPur™ Ni-NTA resin (Thermo Scientific, Waltham, MA). Strep-Tactin affinity chromatography was performed with Strep•Tactin® Superflow™ Agarose (Novagen). Size exclusion chromatography was performed

on a Superdex 200 16/600 or Superdex 200 10/300 GL size-exclusion column (GE Healthcare) attached to an AKTA FPLC system from GE Healthcare (Waukesha, WI) equipped with a P-920 pump and UPC-900 monitor. SDS-PAGE gels and Tris-HCl running buffers were prepared as per Sambrook and Russell [7]. Protein molecular weight standards were obtained from Bio-Rad (Hercules, CA). Analytical reversed phase HPLC (RP-HPLC) was performed on a Varian ProStar instrument with a Vydac C18 column (5 micron, 4 x 150 mm), employing 0.1% trifluoroacetic acid (TFA) in water (HPLC buffer A), and 90% acetonitrile, 0.1% TFA in water (HPLC buffer B), as the mobile phases. Typical analytical gradients were 0-73% HPLC buffer B over 30 min at a flow rate of 1 mL/min. Preparative scale purifications were conducted on a Vydac C18 (15-20 micron, 50 x 250mm) at a flow rate of 9 mL/min. LC-ESI-MS analysis was conducted on a Bruker Esquire LC-ion trap spectrometer (Billerica, MA) in conjunction with an HP1100 series HPLC (Palo Alto, CA). UV Absorbance measurements were performed on a Nanodrop 2000c Spectrophotometer (Thermo Scientific) for Protein 280 methodology or a Multiskan Spectrum Microplate Spectrophotometer (Thermo Labsystems) for Bradford assay. Amino acid analysis was undertaken at the UC Davis Proteomics Core Facility. ImageJ software (http://rsb.info.nih.gov/ij/) was employed to quantify gels. ^{1}H NMR spectroscopy was performed on a Bruker AV500 spectrometer with a Bruker multinuclear inverse BBI-1H{X}-Z gradient probehead and a base frequency of 500 MHz.

3.4.2 *Construction of overexpression plasmids*

PafA-His$_6$ The *pafA* gene was obtained by PCR from genomic DNA of *Corynebacterium glutamicum* (ATCC 13032) employing the forward primer 5'-GGGAATTCCCATGGGCAGTA CCGTGGAATCCGCA-3' (*NcoI*) and reverse primer 5'-GCCTACGCCTCGAGCTAATGATG ATGATGATGATGACTGCGATAGCTCTCCGCATG-3' (*XhoI*). PafA was cloned with a C-terminal hexahistidine-tag between the *NcoI* and *XhoI* restriction sites in the pET15b vector. The correct gene sequence was confirmed by DNA sequencing using T7 forward and reverse primers.

PanB-His$_6$ The PanB gene was obtained from *M. tuberculosis* genomic DNA by PCR with the forward primer 5'-GGGAATTCCATATGTCTGAGCAGACTATCTATGGGGCC-3' (*Nde1*) and reverse primer 5'-GCCCGCGGATCCCTAGTGATGATGATGATGATGGAAACTGTGTT CGTCAGCGGGGAATACCCCGC-3' (*BamH1*). PanB was cloned with a C-terminal

hexahistidine-tag between the *Nde1* and *BamH1* restriction sites in the pE3a vector. The correct gene sequence was confirmed by DNA sequencing using T7 forward and reverse primers.

His_6-strep-PupE Herwin Darwin (NYU) generously donated the plamid of the His_6-strep-PupE-stop-PafA gene sequence from *M. tuberculosis* in a pET24b vector. Two stop codons were inserted in the PafA gene using the QuikChange® Site-Directed Mutagensis Kit (Agilent), so that only His_6-strep-PupE would be obtained during purification. The correct gene sequence was confirmed by DNA sequencing using T7 forward primer.

3.4.3 *General method for the expression and purification of proteins*

All proteins were expressed in *E. coli* BL21 (DE3) cells from isopropyl β-D-1-thiogalactopyranoside (IPTG) inducible plasmids. Cells were grown in LB media (25 g/L) with Ampicillin (100 μg/ml), or Kanamycin (30 μg/ml) *Mtb* strep-Pup, in 3 L baffled-flasks at 37°C until they reached the OD_{600} of 0.5 – 0.7. *Cglu* PafA and *Mtb* PanB protein expression was induced with 0.15 mM IPTG, *Mtb* strep-Pup expression was induced with 0.3 mM IPTG. The induced *Cglu* PafA and *Mtb* PanB cultures were grown for an additional 20 hours at 16 °C and *Mtb* strep-Pup for 5 hours at 25 °C. Cells were harvested by centrifugation at 6000xg for 20 min at 4 °C, and the cell pellet was resuspended cell lysis buffer consisting of 50 mM Tris, 300 mM NaCl, 1 mM β-mercaptoethanol, 10% (v/v) glycerol, pH 7.5 at 4 °C. Cells were lysed by sonication at a pulsed 40% duty cycle for three to four, 3-minute periods on ice. The insoluble cellular debris was cleared by centrifugation at 13,000x*g* for 30 min, followed by filtration of the supernatant through a 0.45 μm filter under vacuum. The filtrate containing the His_6-tagged protein was loaded by gravity flow over 5-10 mL HisPur^{TM} Ni-NTA resin pre-equilibrated with lysis buffer. The column was washed with ten column volumes each of lysis buffer containing 0mM, 50 mM, and 100mM imidazole. Protein was eluted from the column with lysis buffer at 500 mM imidazole. Protein containing fractions were identified by 12% or 15% SDS-PAGE and combined for further purification.

Ni^{2+}-column eluates containing *Cglu* PafA and *Mtb* PanB were concentrated in 10 kDa and 3 kDa MWCO Vivaspin 20 centrifugal filters, respectively. Concentrated samples were purified by S200 size-exclusion chromatography on a Superdex 200 16/600 size-exclusion column (GE Healthcare) attached to the AKTA FPLC system. The elution buffer contained 50

mM Tris, 300 mM NaCl, 1 mM EDTA, 1 mM DTT, and 10% (v/v) glycerol, pH 7.5 at 4 °C. The purity of the resulting peak was assessed by 12% SDS-PAGE, pure samples were concentrated further, and concentration was determined by Bradford protein assay from Thermo Scientific.

Ni^{2+}-column eluate containing Mtb Pup was dialyzed into water for three hours using 3.5 kDa dialysis membrane. The eluate volume was then reduced below 10 mL by vacuum centrifuge, and the lyophilized sample was purified by preparative C18 RP-HPLC using a gradient of 35-70% buffer B over 60 min. The identity of the protein was analyzed by ESI-MS. Protein concentration was estimated from Abs_{280} measurements using a calculated extinction coefficient (ε) of 6990 M-1 cm-1 (ExPASy ProtParam).

3.4.4 *General procedure for pupylation assay and purification of pupylated enzyme*

Pupylation assays were undertaken with 100 μM ATP, 50 μM *Mtb* strep-PupE, 40 μM *Mtb* PanB, and 10 μM *Cglu* PafA in a 500 μL volume. The reaction buffer consisted of 50 mM Tris, 300 mM NaCl, 1 mM DTT, 20 mM $MgCl_2$, and 10% (v/v) glycerol at pH 7.6. The reaction was initiated by the addition of PafA and incubated at 37 °C for 14 hours. Four assays of 500 μL were performed at once, and at the end of the 14 hours, loaded by gravity flow over 1 mL Strep-Tactin Superflow Agarose pre-equilibrated with wash buffer (100 mM Tris, 150 mM NaCl, 1 mM EDTA, pH 8.0). The column was washed with 7 column volumes of wash buffer, and protein was eluted with 8 column volumes of wash buffer with 2.5 mM d-Desthiobiotin. Protein containing fractions were identified by 12% SDS-PAGE, combined, and concentrated in a 3 kDa MWCO Vivaspin 20 centrifugal filter over the course of 4.5 hours. Concentrated samples were purified by S200 size-exclusion chromatography on a Superdex 200 10/300 size-exclusion column (GE Healthcare) attached to the AKTA FPLC system. The elution buffer contained 50 mM Tris, 300 mM NaCl, 1 mM EDTA, 1 mM DTT, and 10% (v/v) glycerol, pH 7.5 at 4 °C. The purity of the resulting peak was assessed by 12% SDS-PAGE, and clean samples were concentrated further in a 3 kDa MWCO Vivaspin 500 centrifugal filter. The S200 elution buffer containing concentrated pupylated protein was exchanged for 1 mM Tris-d_{11} in D_2O for use in NMR measurements using Protein Desalting Spin Columns by (Thermo Scientific). The concentration of pupylated protein in the new buffer was determined using BSA standards run in a 12% SDS-PAGE gel. The density of the Pup-PanB and BSA standard bands were analyzed

using ImageJ software. The concentration of Pup-PanB was then diluted to 20 μM using additional 1 mM Tris-d_{11} in D_2O and stored in aliquots at -80 °C for use in ^1H NMR spectroscopy.

3.4.5 *General procedure for the treatment and purification of unpupylated enzyme*

Careful consideration was taken to ensure the population of unpupylated PanB was treated in the same manner as the pupylated population, so that any difference in observed catalytic activity could be isolated to the presence of Pup, not differences in the purification process. Negative control assays were undertaken, in exclusion of *Mtb* strep-Pup, with 100 μM ATP, 40 μM *Mtb* PanB, and 10 μM *Cglu* PafA in a 500 μL volume. The buffer consisted of 50 mM Tris, 300 mM NaCl, 1 mM DTT, 20 mM $MgCl_2$, and 10% (v/v) glycerol at pH 7.6. Four assays of 500 μL were performed at once and incubated at 37 °C for 14 hours. The assays were combined and treated with 500 μL of a 5x d-Desthiobiotin stock, for exposure to a 2.5 mM concentration. The treated sample was concentrated in a 3 kDa MWCO Vivaspin 20 centrifugal filter over the course of 4.5 hours. Concentrated sample was purified by S200 size-exclusion chromatography on a Superdex 200 10/300 size-exclusion column (GE Healthcare) attached to the AKTA FPLC system. The elution buffer contained 50 mM Tris, 300 mM NaCl, 1 mM EDTA, 1 mM DTT, and 10% (v/v) glycerol, pH 7.5 at 4 °C. The purity of the resulting peak was assessed by 12% SDS-PAGE, and clean samples were concentrated further in a 3 kDa MWCO Vivaspin 500 centrifugal filter. The S200 elution buffer containing concentrated protein was exchanged for 1 mM Tris-d_{11} in D_2O using Protein Desalting Spin Columns by (Thermo Scientific). The concentration of unpupylated protein in the new buffer was determined using BSA standards run in a 12% SDS-PAGE gel. The density of the PanB and BSA standard bands were analyzed using ImageJ software. The concentration of PanB was then diluted to 20 μM using additional 1 mM Tris-d_{11} in D_2O and stored in aliquots at -80 °C for use in ^1H NMR spectroscopy.

3.4.6 *General procedure for measuring PanB and Pup-PanB activity*

Enolization rates were determined by monitoring the exchange of the β-hydrogen of α-ketoisovalerate in D_2O. Solutions for the NMR enolization studies contained 1 mM Tris-d_{11}, 4 mM $MgCl_2$, 100 mM α-ketoisovalerate, and 0.15% (v/v) acetonitrile at pH 7.0, and the reactions were initiated by the addition of 2 μM PanB or Pup-PanB in a total volume of 200 μL. Proton NMR spectra were acquired every 5 min at 25°C on a Bruker AV500 spectrometer at 500 MHz. Kinetic data was obtained by calculating the integrated intensity of the septet centered at 2.95 ppm corresponding to the β-proton relative to the integrated intensity of acetonitrile peak centered at 2.0 ppm. Data from the first hour, estimated to be approximately 10% conversion to product, was used to determine an initial linear rate of hydrogen exchange, k_{ex}. An observed rate of the reaction was calculated using Eqn 3.1,

$$k_{obs} = (k_{ex}\,\mathrm{min}^{-1})[S_i]/[E] \tag{3.1}$$

where $[S_i]$ was the initial substrate concentration and [E] was the enzyme concentration.

The rate of ketopantoate formation was determined by monitoring the appearance of the methyl groups or C4 hydrogens of ketopantoate. Solutions for the NMR ketopantoate formation studies contained 1 mM Tris-d_{11}, 4 mM $MgCl_2$, 100 mM α-ketoisovalerate, 25 mM formaldehyde, 200 μM tetrahydrofolate (not included in the MTHF-independent reaction), and 0.15% (v/v) acetonitrile at pH 7.0, and the reactions were initiated by the addition of 2 μM PanB or Pup-PanB in a total volume of 200 μL. Proton NMR spectra were acquired every 5 min at 25°C on a Bruker AV500 spectrometer at 500 MHz. Kinetic data was obtained by calculating the integrated intensity of the singlet centered at 1.11 ppm corresponding to the methyl groups of ketopantoate or the singlet centered at 3.56 ppm corresponding to the C4 hydrogens relative to the integrated intensity of acetonitrile peak centered at 2.0 ppm. Data from the first hour was fit to Eqn 3.1, as described above, to determine the observed rate of reaction.

3.5 REFERENCES

[1] Samanovic, M. I.; Tu, S.; Novak, O.; Iyer, L. M.; McAllister, F. E.; Aravind, L.; Gygi, S. P.; Hubbard, S. R.; Strnad, M.; Darwin, K. H. (**2015**) Proteasomal control of cytokinin synthesis protects Mycobacterium tuberculosis against nitric oxide, *Mol. Cell* 57, 984.

[2] Tung, C. W. (**2012**) PupDB: a database of pupylated proteins, *BMC Bioinf.* 13, 40.

[3] Sugantino, M.; Zheng, R.; Yu, M.; Blanchard, J. S. (**2003**) Mycobacterium tuberculosis ketopantoate hydroxymethyltransferase: tetrahydrofolate-independent hydroxymethyl transferase and enolization reactions with alpha-keto acids, Biochemistry 42, 191.

[4] Marrakchi, H.; Laneelle, M. A.; Daffe, M. (**2014**) Mycolic acids: structures, biosynthesis, and beyond, *Chem. Biol*. 21, 67.

[5] Delley, C. L.; Striebel, F.; Heydenreich, F. M.; Ozcelik, D. Weber-Ban, E. (**2012**) Activity of the Mycobacterial Proteasomal ATPase Mpa is Reversible Regulated by Pupylation, *J. Biol. Chem.* 287, 7907.

[6] Mondino, S.; Gago, G.; Gramajo, H. (**2013**) Transcriptional regulation of fatty acid biosynthesis in mycobacteria, Mol. Microbiol. 89, 372.

[7] Sambrook, D. W.; Russell, J. (**2001**) Molecular Cloning: a laboratory manual, Third Edition**,** *Cold Spring Harbour Laboratory Press*, Cold Spring Harbour, New York 2100.

DISCLAIMER

The views expressed in this article are those of the author and do not reflect the official policy or position of the United States Air Force, Department of Defense, or the U.S. Government.